Molecular Cancer

RESEARCH

Open Access

Hsa_circ_0125356 promotes gemcitabine resistance by modulating WNT canonical and non-canonical pathways via miR-582-5p/FGF9 axis in non-small cell lung cancer

Xinyue Du[1†], Weijie Luo[1†], Hongwu Li[1], Qi Gu[1], Ping Huang[1], Cheng Wang[1], Na Li[1], Fanglan Liu[1,2*] and Chunhua Xia[1,2*]

Abstract

Background Non-small cell lung cancer (NSCLC) is the leading cause of cancer morbidity and mortality worldwide. The prognosis of patients has been significantly improved by chemotherapy, but acquired drug resistance remains a major obstacle to NSCLC treatment. Circular RNAs (circRNAs), which act as miRNA or protein sponges, are critically associated with the development and chemotherapy resistance of NSCLC.

Methods CircRNA sequencing was performed to analyze the differential expression of circRNAs between A549 and A549-GR cells. Chromogenic in situ hybridization (CISH) and immunohistochemistry (IHC) technologies were used to detect the expression of hsa_circ_0125356, miR-582-5p,and FGF9 in NSCLC tissues and para-carcinoma tissues. Fluorescence in situ hybridization (FISH), dual-luciferase reporter assays and RNA immunoprecipitation (RIP) were conducted to evaluate the expression and regulation of hsa_circ_0125356, miR-582-5p, and FGF9. Furthermore, the regulation of hsa_circ_0125356/miR-582-5p/FGF9 on gemcitabine sensitivity was confirmed by TUNEL, Transwell, EdU, CCK8 and immunohistochemistry.

Results We identified a novel hsa_circ_0125356 as a therapeutic target against gemcitabine resistance. Hsa_circ_0125356 was significantly elevated in clinical samples of patients with NSCLC. Moreover, hsa_circ_0125356 overexpression promoted gemcitabine resistance to NSCLC by upregulating FGF9 via sponging miR-582-5p in vivo and in vitro. Notably, WNT canonical (ERK/GSK3β/β-catenin) and non-canonical (Daam1/RhoA/ROCK2) signaling pathways were activated due to hsa_circ_0125356 acting as an endogenous miR-582-5p sponge to regulate the expression of FGF9, and thereby enhancing gemcitabine resistance via promoting DNA damage repair and inhibition of apoptosis. The results were further confirmed by two small molecule antagonists, WAY 316606 and XAV-939,which could inhibit the activation of WNT signaling pathway induced by hsa_circ_0125356.

Conclusion We first demonstrated that hsa_circ_0125356 was significantly upregulated and served as a biomarker for gemcitabine resistance in NSCLC by sponging miR-582-5p/FGF9 axis to regulate the WNT canonical

[†]Xinyue Du and Weijie Luo contributed equally to this work.

*Correspondence:
Fanglan Liu
liufanglan@ncu.edu.cn
Chunhua Xia
xch720917@ncu.edu.cn
Full list of author information is available at the end of the article

and non-canonical signaling pathways, which provided a new direction for identification of therapeutic targets for the treatment of gemcitabine resistance of NSCLC.

Keywords CircRNAs, NSCLC, Gemcitabine resistance, MiR-582-5p, FGF9, WNT canonical and non-canonical signaling pathways

Introduction

Non-small cell lung cancer (NSCLC) accounts for approximately 40–55% of primary lung cancer cases, and its incidence has increased in recent years, representing a serious threat to human health [1, 2]. At present, surgery-based comprehensive treatment remains the primary treatment mode for NSCLC, but it still has a high rate of recurrence and distant metastasis [3, 4]. Chemotherapy has been widely used in the treatment of patients with unresectable and postoperative recurrent NSCLC. However, the emergence of chemoresistance poses a significant challenge to the efficacy of chemotherapy, eventually leading to poor prognosis [5, 6].

Gemcitabine, a pyrimidine nucleoside analog with a broad spectrum of antitumor activity, is one of the most commonly used chemotherapeutic agents for the clinical treatment of NSCLC [7]. Gemcitabine in combination with other chemotherapeutic agents is a recognized first-line chemotherapy regimen in the treatment of advanced NSCLC. For instance, gemcitabine in combination with cisplatin and sintilimab reveals preliminary efficacy and manageable safety as a first-line therapy for patients with squamous NSCLC, with an objective response rate of 64.7% and a median progression-free survival of 6.5 months [8]. The combination therapy of gemcitabine and docetaxel for lung adenocarcinoma results in a median time to progression of 4.1 months, a median overall survival of 9.4 months, and 1-year and 2-year survival rates of 37.9% and 10.7%, respectively [9]. Moreover, the co-administration of gemcitabine and docetaxel is considered as an effective and well-tolerated regimen for the treatment of NSCLC, especially in patients with adenocarcinoma NSCLC with a higher overall response rate of 43% [10]. However, gemcitabine resistance has continued to limit our ability to effectively treat advanced NSCLC. A growing body of evidence underscores that gemcitabine resistance may result from alterations in drug metabolism until the cytidine analog is incorporated into the DNA, or from mitigation of gemcitabine-induced apoptosis [11, 12]. These drug resistance modalities can be intrinsic to cancer cells or influenced by the cancer microenvironment. Moreover, the underlying mechanisms of gemcitabine resistance are difficult to address, as many genes that drive the carcinogenic process themselves also interfere with gemcitabine-induced apoptosis [13]. In recent years, several studies have reported that circular RNA (circRNA) is a novel biomarker and therapeutic target, providing further insight into gemcitabine resistance in cancer therapy.

CircRNA is recognized as a class of functional non-coding RNAs (ncRNAs) that connects the downstream 5' site with the upstream 3' site to form a covalently closed single-stranded loop [14]. CircRNA regulates biological processes by mediating alternative splicing of RNA, cis-regulation of transcription, and functioning as a competitive endogenous RNA (ceRNA) [15, 16]. A growing body of evidence suggests that circRNA plays a critical role in various cancer-related processes, including tumorigenesis, metastasis, recurrence, and drug resistance [17–19]. The abnormal expression of circRNA is closely related to the occurrence and development of lung cancer. For instance, hsa_circHIPK3 promotes lung cancer cell proliferation by sponging miR-124/CDK4 axis [20]. The downregulation of hsa_circ_0006427 inhibited metastasis of NSCLC by regulating miR-6783-3p/DKK1 signaling pathway [21]. A newly emerging mechanism underlies that hsa_circ_0035483 promotes the resistance of human renal cancer cells to gemcitabine by modulating autophagy activation via sponging hsa-miR-335 [22]. Hsa_circ_103809 enhances gemcitabine resistance by activating miR-516-5p/FBXL18 axis in bladder cancer cells [23]. However, the role of circRNAs in the gemcitabine resistance of NSCLC is still not well understood.

In summary, circRNA plays a crucial regulatory role in the occurrence, development, and resistance of chemotherapy in NSCLC. However, the correlation between circRNAs and gemcitabine resistance in NSCLC, along with its functional roles and mechanisms, remains poorly studied. The main objectives of the present study were to explore the impact of circRNAs on gemcitabine resistance in NSCLC and its underlying mechanisms. Our findings will provide clinical significance in

understanding the molecular mechanisms of gemcitabine resistance in NSCLC and in devising a novel therapeutic target for chemotherapy resistance in NSCLC.

Materials and methods

Patient information and tissue specimens

Sixty-four tissues from patients with NSCLC and sixty-four adjacent tissues, which were histopathologically and clinically diagnosed, were obtained from the First People's Hospital of Jiujiang, Jiangxi Province. All experiments involving human samples and clinical data were approved by the Ethics Committee of Jiujiang First People's Hospital (Ethics NO: JSDYRMYY-YXLL-2024–300).

Immunohistochemistry (IHC)

For immunohistochemical staining, all paraffin-embedded tissues were soaked in xylene and different concentrations of alcohol for deparaffinization and hydration. After antigen repair, the tissues were incubated in 3% H_2O_2 (Boster Biotech, CA, USA) at room temperature in the dark for 10 min, before adding 5% bovine serum albumin (BSA) (Solarbio, Beijing, China) at room temperature for 1 h. Slides were prepared with primary antibodies targeting fibroblast growth factor 9 (FGF9) (YT5179, Immunoway, USA, 1:1000) and Ki67 (ab16667, Abcam, UK, 1:1000) overnight at 4 °C. The next day, the slides were incubated with a secondary antibody for 1 h at room temperature and then stained with diaminobenzidine (Servicebio, Wuhan, China). Finally, the slides were covered with coverslips, sealed with neutral gum, and viewed under a fluorescence microscope. Cell staining intensity was scored as follows: 0, points for no positive staining (negative); 1, light yellow (weak positive); 2, brown yellow (positive); and 3 points for tan (strong positive). The positive rate of tumor cells was scored as follows: 1, 0%–25%; 2, 26%–50%; 3, 51%–75%; and 4, 76%–100%.

Establishment of cell lines and transfection

Human NSCLC cells (lung adenocarcinoma: A549, HCC827, SKMES1, SPCA1, H1299, H292 and lung squamous cell carcinoma: H520) were purchased from the American Type Culture Collection (ATCC, USA). Gemcitabine-resistant A549 (A549-GR) cells were obtained from Shanghai Meixuan Biotechnology Co., Ltd. (Shanghai, China). Transfection of hsa_circ_0125356, si-hsa_circ_0125356, miR-582-5p mimics, inhibitors, overexpressed Flag-FGF9 plasmids (OE-FGF9), FGF9-specific shRNAs (shFGF9), or the corresponding NCs into cells was performed using lipofectamine 3000 (Uelandy, Suzhou, China). Lentiviral shRNAs and overexpression constructs were generated by Genechem (Guangzhou, China). The cells were transfected with lentivirus according to the manufacturer's instructions. The sequences used are listed in Supplementary Table S1.

RNase R treatment

RNase R was applied to digest linear RNA. RNAs extracted from A549 and A549-GR cells were divided into two groups for RNase R (Geneseed, Guangzhou, China) treatment and control. The samples were incubated for 30 min at 37 °C with 3 U/μg of RNase R. Quantitative real-time PCR (qRT-PCR) was used to detect the expression of SLC7A11 and hsa_circ_0125356. GAPDH in the control group was used as the internal reference. Three independent experiments were performed in triplicate. All primers are listed in Supplementary Table S2.

Actinomycin D (ActD) treatment

A total of 1×10^5 cells per well of A549 and A549-GR cells were seeded in a 6-well plate overnight, and 2 mg/L ActD (MCE, New Jersey, USA) was added to each well for 4, 8, 12, and 24 h. The cells were harvested according to treatment time. qRT-PCR was performed to analyze the stability of SLC7A11 mRNA and hsa_circ_0125356. Three independent experiments were performed in triplicate.

Cell viability analysis

Cells with or without transfection were seeded in 96-well plates at 5×10^3 cells/well for 24 h and then treated with different concentrations of gemcitabine for 48 h. Cell viability was measured using a CCK-8 Assay Kit (Dojindo, Kanto Area, Japan) to measure the cytotoxicity of gemcitabine. The half-maximal inhibitory concentration (IC_{50}) was determined based on the absorbance at 490 nm, as measured using a microplate reader.

5-Ethynyl-2′-deoxyuridine (EdU) incorporation assay

A cell-light EdU DNA cell proliferation kit (Uelandy, Suzhou, China) was used to perform the EdU assay. After incubation with 50 mM EdU for 2 h, the A549 and A549-GR cells were fixed in 4% paraformaldehyde and stained with Apollo Dye solution. Hoechst 33,342 was used to identify the nuclei. The proliferation-positive cells were then photographed and counted under an Olympus FSX100 microscope.

Colony formation assays

A549 and A549-GR cells were resuspended to 1×10^3 cells/mL and seeded in 6-well plates. After incubation at 37 °C

for 14 days, cells were fixed in methanol (Sinopharm, Beijing, China), stained with 0.1% crystal violet (Solarbio, Beijing, China) and the cell colonies were counted.

Migration assays

Transwell migration assays were performed. Transfected A549 and A549-GR cells (1×10^6 cells/mL) were resuspended in RPMI 1640 medium (solarbio, Beijing, China). The upper chamber contained 100 µL of cell suspension medium, and 600 µL of complete medium was added to the bottom chamber. After incubating at 37 °C in an atmosphere containing 5% CO_2 for 24 h, the cells were fixed with 4% paraformaldehyde and stained with 0.1% crystal violet solution. The cells that passed through the filter were photographed and counted by inverted fluorescence microscopy in three randomly selected fields.

Apoptosis analysis

According to the manufacturer's instructions of flow cytometry kit (Uelandy, Suzhou, China), apoptosis was measured using a flow cytometer (FACSCalibur, BD, USA). After 48 h of treatment, the cells were washed, resuspended, and stained with fluorescein isothiocyanate and propidium iodide. Subsequently, flow cytometry was used to analyze the apoptosis rate of cells treated under different conditions. The apoptosis data were analyzed using FlowJo V10 software (Tree Star, San Francisco, USA). Each experiment was performed more than three times.

Fluorescence in situ hybridization (FISH)

A Cy3-labeled oligonucleotide probe (IbsBio, Shanghai, China) targeting hsa_circ_0125356 was used for FISH (Ribobio, Guangzhou, China) (sequence shown in Supplementary Table S1). Cells were seeded in confocal dishes and incubated with pre-hybridization solution at 37 °C for 30 min. 20 µM probes were added to the dish and hybridized overnight. After washing (4×SSC (saline sodium citrate in 0.1% Tween-20) three times, 2×SSC once, and 1×SSC once), the cells were stained with 4', 6-diamidino-2-phenylindole (DAPI) for 15 min at room temperature. Finally, images were observed under a confocal microscope.

ELISAs

A549, HCC827, SKMES1, SPCA1, H1299, H292 and A549-GR cells were cultured in large dishes. Meanwhile, the blank group and the basal medium group were set up. On day 3 of cultivation, the cell supernatant was collected for measuring FGF9 content according to the instructions of the ELISAs kit (EIAAB, Wuhan, China).

In situ hybridization (ISH)

The steps for deparaffinization and rehydration were the same as those for ICH, and the sections were digested with proteinase K (Servicebio, Wuhan, China) after heat repair and then hybridized with digoxigenin-labeled probes (IbsBio, Shanghai, China) overnight at 37 °C. Next, the HRP digoxin antibody was labeled, the color was developed with diaminobenzidine, nuclei were counterstained, and slides were sealed by dehydration. The sections were observed using standard light-field microscopy. The target probe showed brownish punctate or clump-like signals in the cells, and the nucleus was dark blue.

In vivo animal experiments

To investigate the effects of hsa_circ_0125356 in vivo, 1×10^7 A549-GR cells (n = 5 in each group) stably transfected with hsa_circ_0125356 shRNA or NC and 1×10^7 A549 cells (n = 5 in each group) stably transfected with overexpression of hsa_circ_0125356 or vector were injected subcutaneously into the flanks of 4-week-old BALB/c nude mice (Gempharmatech, Nanjing, China).

(See figure on next page.)

Fig. 1 Identification of gemcitabine resistance-associated circRNA (hsa_circ_0125356) in NSCLC after gemcitabine treatment. **A** High throughput circRNA sequencing analysis of circRNA expression profiling in A549 and A549-GR cells. **B** qRT-PCR indicating the levels of 12 differentially expressed circRNAs in A549 and A549-GR cell lines. **C** PCR analysis of hsa_circ_0125356 and the linear transcript of SLC7A11 using divergent and convergent primers in cDNA and genomic DNA (gDNA). GAPDH was used as a control. **D** Schematic of the chromosomal location and formation of hsa_circ_0125356. Sanger sequencing was used to verify the splice junctions. **E** qRT-PCR analysis of hsa_circ_0125356 using random primers or oligo DT primers in reverse transcription experiments. **F** Relative RNA levels of hsa_circ_0125356 and linear SLC7A11 treated with RNase R. **G** Relative abundance of hsa_circ_0125356 and linear SLC7A11 treated with actinomycin D at the indicated time points. **H**, **I** The subcellular localization of hsa_circ_0125356 in A549-GR cells was determined by nuclear mass separation assay and fluorescence in situ hybridization. GAPDH and 18S represent cytoplasmic controls, and U6 represents nuclear controls. Scale bar: 10 µm. **J** In situ hybridization was used to detect the differential expression of hsa_circ_0125356 in paired tumor/paracarcinoma tissue samples from 64 NSCLC patients. Scale bar: 50 µm. **K** Kaplan–Meier analysis of the correlation between hsa_circ_0125356 expression and overall survival (OS) for NSCLC patients. Data are shown as the mean ± SD. $^{*}P<0.05$; $^{**}P<0.01$; $^{***}P<0.001$; $^{****}P<0.0001$

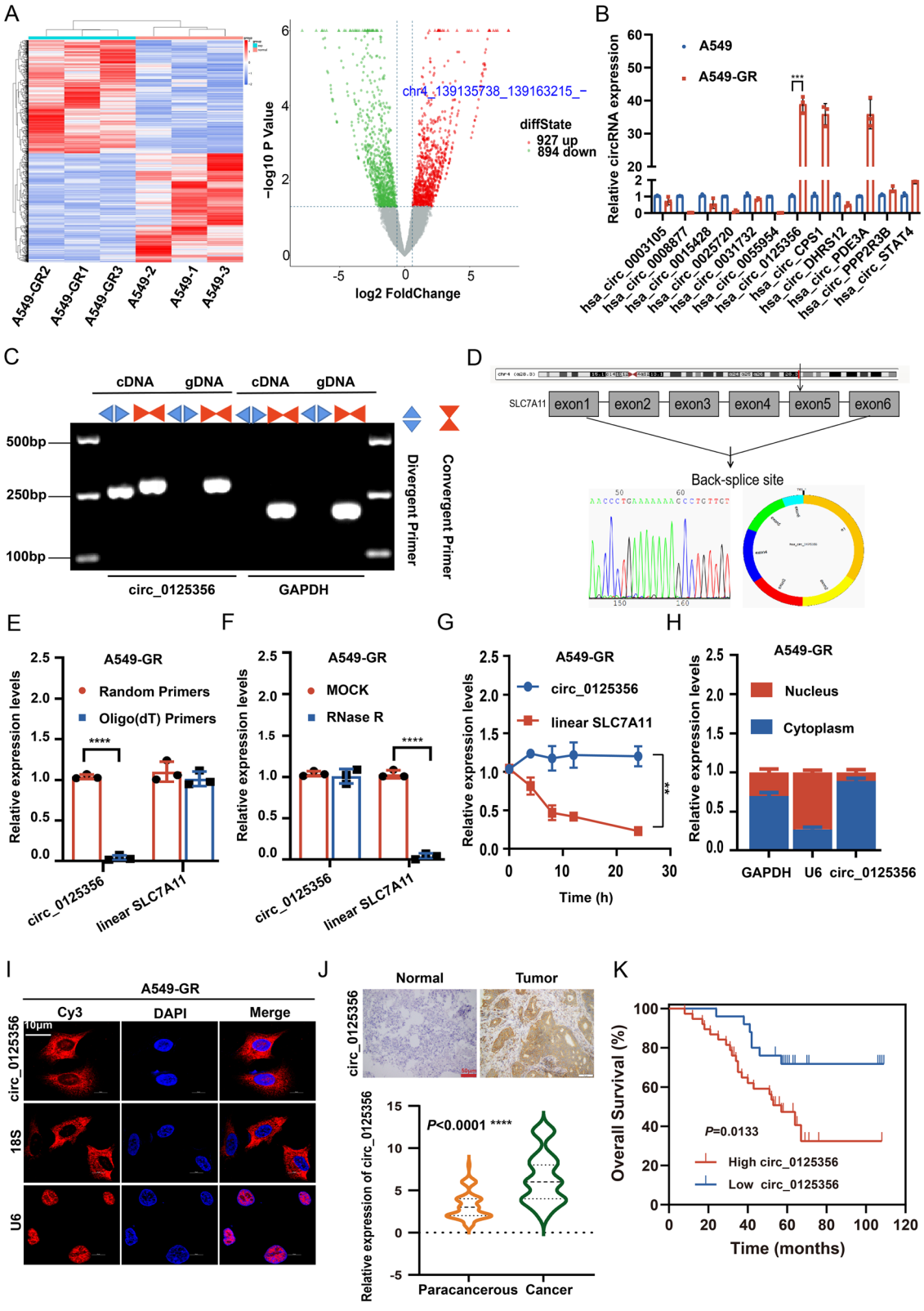

Fig. 1 (See legend on previous page.)

Two weeks after injection, the animals were randomly assigned to the vehicle control or gemcitabine (50 mg/kg) group, and gemcitabine was injected intraperitoneally every 3 days. Mice were euthanized in the sixth week, and tumors were isolated for further analyses. The subcutaneous tumor size was measured and recorded every 2 days using a vernier caliper: tumor volume (mm^3) = $(L \times W^2)/2$, where L is the long axis and W is the short axis. All animal care and experimental procedures were performed in accordance with the Guidelines for the Care and Use of Laboratory Animals issued by NIH, and the animal experimental protocol was approved by the Ethics Committee of Nanchang University (Animal Ethics batch No.: NCULAE-20240530001).

CircRNA sequencing technology

In this study, the NSCLC parental strain and NSCLC gemcitabine-resistant strain were first used for library construction using a Clontech SMARTer Stranded Total RNA-seq kit v2-Pico Input kit (Takara, Kyoto, Japan) to screen differentially expressed circRNAs. After constructing the library, Qubit 3.0 was used for preliminary quantification, and then an Agilent 2100 Bioanalyzer was used to detect the library size range. The effective concentration of the library was accurately quantified by q-PCR (effective concentration > 3 nM) to ensure the quality of the library. The circRNA libraries were pooled according to the requirements of effective concentration and target data volume and sequenced using a Nova-seq 6000 PE150 mode (Geneseed, Guangzhou, China). The circRNA-seq raw data (raw reads) of fastq format were firstly processed through in-house Perl scripts. Index of the reference genome was built using Bowtie 2 version 2.1.0, and paired-end clean reads were aligned to the reference genome using Bowtie. Prior to differential gene expression analysis, the reads were mapped to genome using the STAR and DCC was used to identify the cirRNA and to estimate their expression. Differential expression analysis of circRNAs was performed using the edgeR R package. The fold change was log2 transformed, and we used a log2 (fold change) > 2 (or < −2) and a p value < 0.01 to sort the differently expressed circRNAs. Subsequently, to generate an overview of circRNA expression profiles between the two groups, hierarchical clustering analysis was performed.

Nucleic acid extraction and quantitative polymerase chain reaction (qPCR)

Total RNA was extracted using TRIzol (Invitrogen, California, USA) according to the manufacturer's instructions. To generate nuclear and cytoplasmic RNA, a nuclear mass separation assay was performed using an NE-PER Nuclear and Cytoplasmic Extraction kit, followed by TRIzol extraction. Genomic DNA (gDNA) was extracted using a genomic DNA isolation kit (Biomiga, San Diego, USA). Complementary DNA (cDNA) was synthesized using PrimeScript RT Master Mix (Vazyme, Nanjing, China). Polymerase chain reaction (PCR) was performed using GoTaq Green Master Mix (Vazyme, Nanjing, China). PCR products were subjected to electrophoresis and visualized with Safe Green. qRT-PCR analysis was conducted using 2×SYBR Green Pro Taq HS Premix II (TransGen, Beijing, China) on RT-PCR instruments. GAPDH was used as an internal control for circRNAs and mRNAs, while small miRNA levels were normalized to those of small nuclear U6. The $2^{-\Delta\Delta Ct}$ method was used to calculate the relative expression. The primer sequences are provided in Supplementary Table S2.

RNA immunoprecipitation (RIP)

The RIP assay was performed according to the RNA Binding Protein Immunoprecipitation Kit manual (17–700, Millipore, USA). In brief, A549 and A549-GR cells were washed twice with cool phosphate-buffered saline and lysed with RIP buffer. The lysates were first co-incubated with anti-AGO2 (67,934–1-Ig, Proteintech, China) or negative control IgG overnight at 4 °C. Subsequently, the protein A/G beads were co-incubated with the immunocomplex mixture for 2 h at 4 °C. The total RNA of the immunocomplex was extracted using TRIzol reagent, and hsa_circ_0125356 and miR-582-5p expression was detected using qRT-PCR. The primer sequences are listed in Supplementary Table S2.

(See figure on next page.)

Fig. 2 Hsa_circ_0125356 is critical for maintaining gemcitabine resistance. **A** The overexpression and knockdown of hsa_circ_0125356 were confirmed by qRT-PCR analysis of hsa_circ_0125356 and SLC7A11 mRNA in A549 and A549-GR cells. **B-D** The proliferative abilities of stably transfected A549 and A549-GR cells treated with gemcitabine were investigated via CCK-8 assays (cell viability and IC_{50}) and colony formation assays. **E** The proliferative abilities of stably transfected A549 and A549-GR cells treated with gemcitabine were investigated using EdU assays. Scale bar: 20 μm. **F**, **G** TUNEL and Transwell assays were used to detect changes in the apoptosis or migration of stably transfected A549 and A549-GR cells treated with gemcitabine. TUNEL Scale bar: 20 μm. Transwell Scale bar: 50 μm. **H** Western blotting was used to detect the protein expressions of apoptosis-related proteins in stably transfected A549 and A549-GR cells treated with gemcitabine. Data are shown as the mean ± SD. $^{*}P < 0.05$; $^{**}P < 0.01$; $^{***}P < 0.001$; $^{****}P < 0.0001$

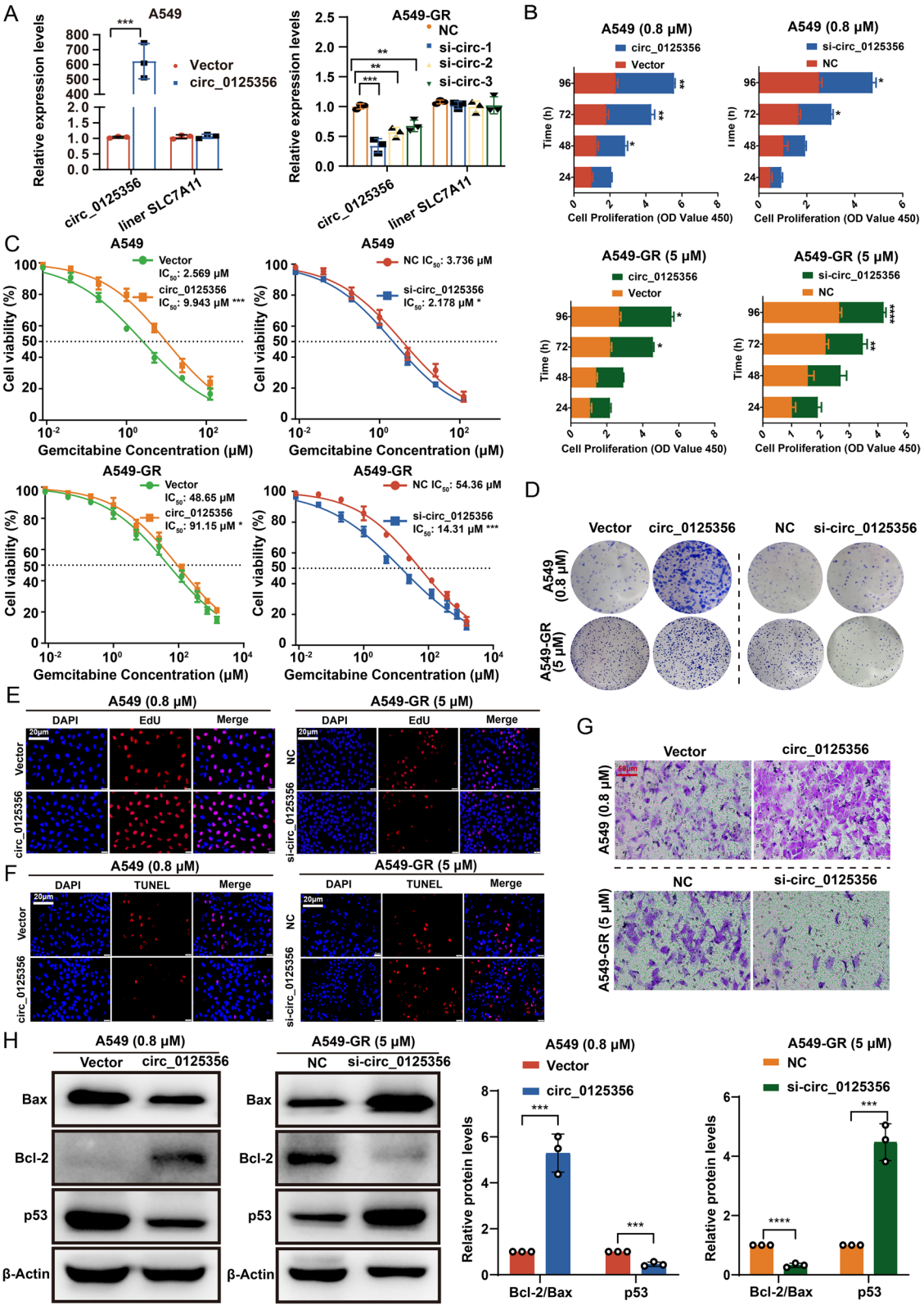

Fig. 2 (See legend on previous page.)

Western blotting analysis

In brief, proteins were isolated from A549 and A549-GR cells using RIPA buffer (89,900, Pierce, USA) supplemented with proteinase inhibitors, and protein concentrations were determined using BCA reagent (30,342, Cwbio, China). Cell lysates were separated on SDS–polyacrylamide gels and then transferred onto polyvinylidene difluoride (PVDF) (Millipore, Schwalbach, Germany). After blocking the membranes in 5% skim powdered milk for 2 h, they were incubated with the following primary antibodies overnight at 4 °C: Ki67 (ab16667, Abcam, UK, 1:1000), Bcl-2 (68,103–1-PBS, Proteintech, China, 1:1000), FGF9 (YT5179, Immunoway, USA, 1:1000), ERK1/2 (A16686, Abclonal, China, 1:1000), p-ERK1/2 (80,031–1-RR, Proteintech, China, 1:1000), β-catenin (51,067–2-AP, Proteintech, China, 1:1000), p-β-catenin (AP0579, Abclonal, China, 1:1000), Gsk3-β (A2081, Abclonal, China, 1:1000), p-Gsk3-β (14,850–1-AP, Proteintech, China, 1:1000), Daam1 (14,876–1-AP, Proteintech, China, 1:1000), RhoA (10,749–1-AP, Proteintech, China, 1:1000), ROCK2 (21,645–1-AP, Proteintech, China, 1:1000), p53 (10,442–1-AP, Proteintech, China, 1:1000), Bax (50,599–2-Ig, Proteintech, China, 1:1000), FGFR3(66,954–1-lg, Proteintech, China, 1:2000), β-actin (HRP-66009, Proteintech, China, 1:6000), and GAPDH (60,004–1-Ig, Proteintech, China, 1:6000). Next, the membranes were incubated with secondary antibodies at room temperature for 1 h. After washing three times, the targeted proteins were visualized using enhanced chemiluminescence (ECL) reagent.

Luciferase reporter assay

A549 and A549-GR cells were seeded in 96-well plates and then co-transfected with hsa_circ_0125356/FGF9 wild-type or mutant plasmids, miR-582-5p mimics, or miR-NC using Lipofectamine 3000. After 48 h of incubation, the luciferase activity was measured according to the manufacturer's instructions (Promega, Madison, USA). Each experiment was repeated at least three times.

Statistical analysis

Data are reported as the means ± standard deviations (SDs), and GraphPad Prism (version 8.0) was used for the general statistical analysis. Differences between the indicated groups were compared using the Student's t-test and one-way analysis of variance (ANOVA). The chi-square test was used to investigate the significance of the correlation of hsa_circ_0125356, miR-582-5p and FGF9 expression with the clinicopathological features. The survival curves were calculated by the Kaplan–Meier method and compared with the log-rank test. Pearson's correlation coefficient was used to evaluate the correlation. A *P*-value less than 0.05 was considered statistically significant.

Results

Discovery and characteristics of novel gemcitabine resistance-related circRNA in NSCLC

A gemcitabine-resistant cell model (A549-GR) was constructed in this study and the CCK-8 assay showed that gemcitabine had a median IC_{50} of 3.344 μM in wild-type cells (A549) and 58.63 μM in A549-GR cells, indicating a resistance index of 19.3 in the A549-GR cell line (Supplementary Fig. S1C). CircRNA sequencing showed that a total of 927 and 894 circRNAs were upregulated and downregulated in A549-GR cells, respectively, compared with wild-type cells (Fig. 1A). Based on log2 (fold change) > 2 (or < −2) and p value < 0.01 (resistant group vs. sensitive group), 12 candidate circRNAs were further selected in A549 and A549-GR cells using qRT-PCR, of which hsa_circ_0125356 was more highly expressed than other candidate circRNAs in A549-GR cells (Fig. 1B).

CircRNAs have the same sequences as the linear transcripts of their parental genes, except for the back-splice junction area [24]. CircRNA sequencing showed that SLC7A11 is the parent host gene of hsa_circ_0125356 (chr4:139,135,738–139,163,215), which was generated from exons 1–6 of the SLC7A11

(See figure on next page.)

Fig. 3 Hsa_circ_0125356 acts as a miRNA sponge for miR-582-5p. **A** Potential target miRNAs of hsa_circ_0125356 were predicted in the Miranda, Circbank, and TargetScan databases. **B** qRT-PCR was used to detect changes in the expression of 12 miRNAs after circRNA overexpression. **C** In situ hybridization was used to detect the miR-582-5p expression differences between 25 patients with NSCLC and 25 patients with paracarcinoma. **D** The negative correlation between hsa_circ_0125356 and miR-582-5p in 25 patients with NSCLC and 25 patients with paracarcinoma was analyzed using Pearson correlation analysis. **E** qRT-PCR was used to detect the expression difference in miR-582-5p between A549 and A549-GR cells. **F** The co-localization of hsa_circ_0125356 (red) and miR-582-5p (green) was observed via fluorescence in situ hybridization (FISH) in A549 and A549-GR cells. Cell nuclei were counterstained with DAPI (blue). Scale bar: 10 μm. **G** RIP assay was performed with anti-AGO2 antibodies or IgG in A549 and A549-GR cells, before performing qRT-PCR to detect the enrichment of hsa_circ_0125356 and miR-582-5p. **H** Luciferase activity of hsa_circ_0125356-WT or hsa_circ_0125356-MUT after transfection with miR-582-5p mimics or inhibitors in A549 and A549-GR cells. **I** qRT-PCR was used to analyze the effect of overexpression or knockdown of hsa_circ_0125356 on miR-582-5p. Data are shown as the mean ± SD. $^{*}P < 0.05$; $^{**}P < 0.01$; $^{***}P < 0.001$; $^{****}P < 0.0001$

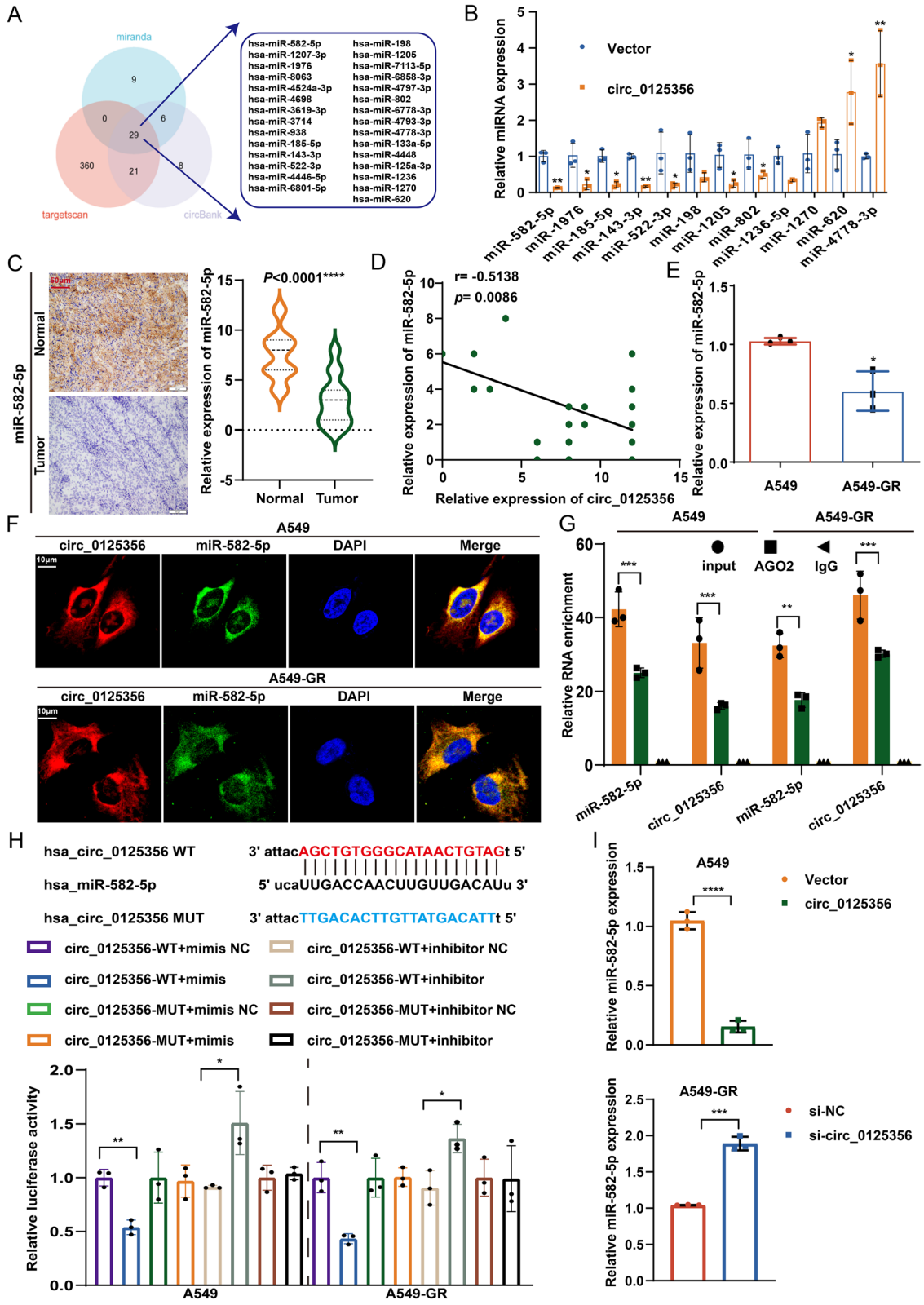

Fig. 3 (See legend on previous page.)

transcript with a length of 783 nt and the mature sequence of hsa_circ_0125356 was list in Supplementary Table S3. Hence, we designed divergent and convergent primers to amplify hsa_circ_0125356 and linear SLC7A11, respectively. The results showed that hsa_circ_0125356 could only be amplified by divergent primers in cDNA but not by gDNA (Fig. 1C). Sanger sequencing directly verified that the splice point matched the junction sequence of hsa_circ_0125356 in circBase (Fig. 1D). We also found that hsa_circ_0125356 could only be reversed using random primers, whereas linear SLC7A11 could be reverse transcribed using random or oligodT primers (Fig. 1E and Supplementary Fig. S2A). Meanwhile, hsa_circ_0125356 was more stable than SLC7A11 mRNA after treatment with RNase R (Fig. 1F and Supplementary Fig. S2B). After treating the cells with ActD (a transcription inhibitor), we found that hsa_circ_0125356 was more stable than linear SLC7A11 (Fig. 1G, Supplementary Fig. S2C). In addition, qRT-PCR and FISH were performed to determine the intracellular location of hsa_circ_0125356 in NSCLC cells, and the results demonstrated that hsa_circ_0125356 was mainly located in the cytoplasm (Fig. 1H&I and Supplementary Fig. S2D&E). Interestingly, the expression of hsa_circ_0125356 was gradually increased due to the enhanced resistance of gemcitabine in A549 cells (Supplementary Fig. S1). Moreover, the clinical data of 64 paired tumor/adjacent tissue samples from patients with adenocarcinoma NSCLC showed that hsa_circ_0125356 was significantly upregulated in cancer tissues compared to adjacent normal tissues (Fig. 1J), and strong expression of hsa_circ_0125356 was significantly associated with higher histologic grade (Supplementary Table S4). Moreover, we analyzed the relationship between the expression of hsa_circ_0125356 and prognosis of NSCLC. The results showed that higher expression of hsa_circ_0125356 predicted poorer survival outcomes in NSCLC (Fig. 1K). These results indicate that hsa_circ_0125356 is a stable and mainly cytoplasmic circRNA that might be involved in tumor progression and drug resistance in NSCLC.

CircRNA-0125356 promoted gemcitabine resistance in NSCLC cells

We effectively silenced hsa_circ_0125356 through siRNA and overexpressed hsa_circ_0125356 using plasmids in both A549 and A549-GR cell lines. As shown in results (Fig. 2A and Supplementary Fig. S3A&B), neither the silencing nor overexpression of hsa_circ_0125356 influenced the expression of linear SLC7A11 mRNA. In the absence of gemcitabine treatment, overexpressed or silencing circ_0125356 barely affected the proliferation and migration abilities of A549 and A549-GR cells compared with the control group (Supplementary Fig. S4A-C). However, in the presence of gemcitabine, hsa_circ_0125356 interference markedly inhibited the viability of A549-GR cells and partially reversed drug resistance, whereas hsa_circ_0125356 overexpression notably increased the viability of A549 cells (Fig. 2B&C). Similar results were also confirmed by colony formation assays (Fig. 2D). Thus, we focused on hsa_circ_0125356 interference in A549 GR cells and hsa_circ_0125356 overexpression in A549 cells. EdU assays were performed to confirm that hsa_circ_0125356 promoted proliferation of A549 cells and A549-GR cells after gemcitabine treatment (Fig. 2E). TUNEL staining further demonstrated that hsa_circ_0125356 knockdown triggered the induction of apoptosis after gemcitabine treatment in A549-GR cells, whereas the number of apoptotic cells was decreased significantly after hsa_circ_0125356 overexpression in A549 cells (Fig. 2F). Cell migration assays also indicated that silencing hsa_circ_0125356 inhibited the migration ability of A549-GR cells with gemcitabine treatment, whereas overexpressing hsa_circ_0125356 obviously increased the migration ability of A549 cells (Fig. 2G). Furthermore, apoptosis-related proteins were detected by western blotting, and the results illustrated that the overexpression of hsa_circ_0125356 dramatically activated the protein expression of Bax, Bcl-2 and p53 in A549 cells, whereas downregulation of hsa_circ_0125356 obviously reversed the expression of Bax, Bcl-2 and p53 in A549-GR cells after gemcitabine treatment (Fig. 2H). Similar phenomena were also observed in the H520 cells (Supplementary Fig. S5). These results provided further evidence that hsa_circ_0125356 promoted the

(See figure on next page.)

Fig. 4 MiR-582-5p reverses gemcitabine resistance of hsa_circ_0125356. **A** The changes in sensitivity to gemcitabine in A549 and A549-GR cells transfected with miR-582-5p mimics and miR-582-5p inhibitor or co-transfected with overexpressed or knocked down hsa_circ_0125356 were investigated using the CCK-8 assay (IC_{50}). **B–D** Colony formation, CCK-8, and EdU assays were used to detect changes in the proliferation of stably transfected A549 and A549-GR cells treated with gemcitabine. Scale bar: 20 μm. **E** Transwell assays were used to detect changes in migration of stably transfected A549 and A549-GR cells treated with gemcitabine. Scale bar: 50 μm. Data are shown as the mean ± SD. $^{*}P < 0.05$; $^{**}P < 0.01$; $^{***}P < 0.001$; $^{****}P < 0.0001$

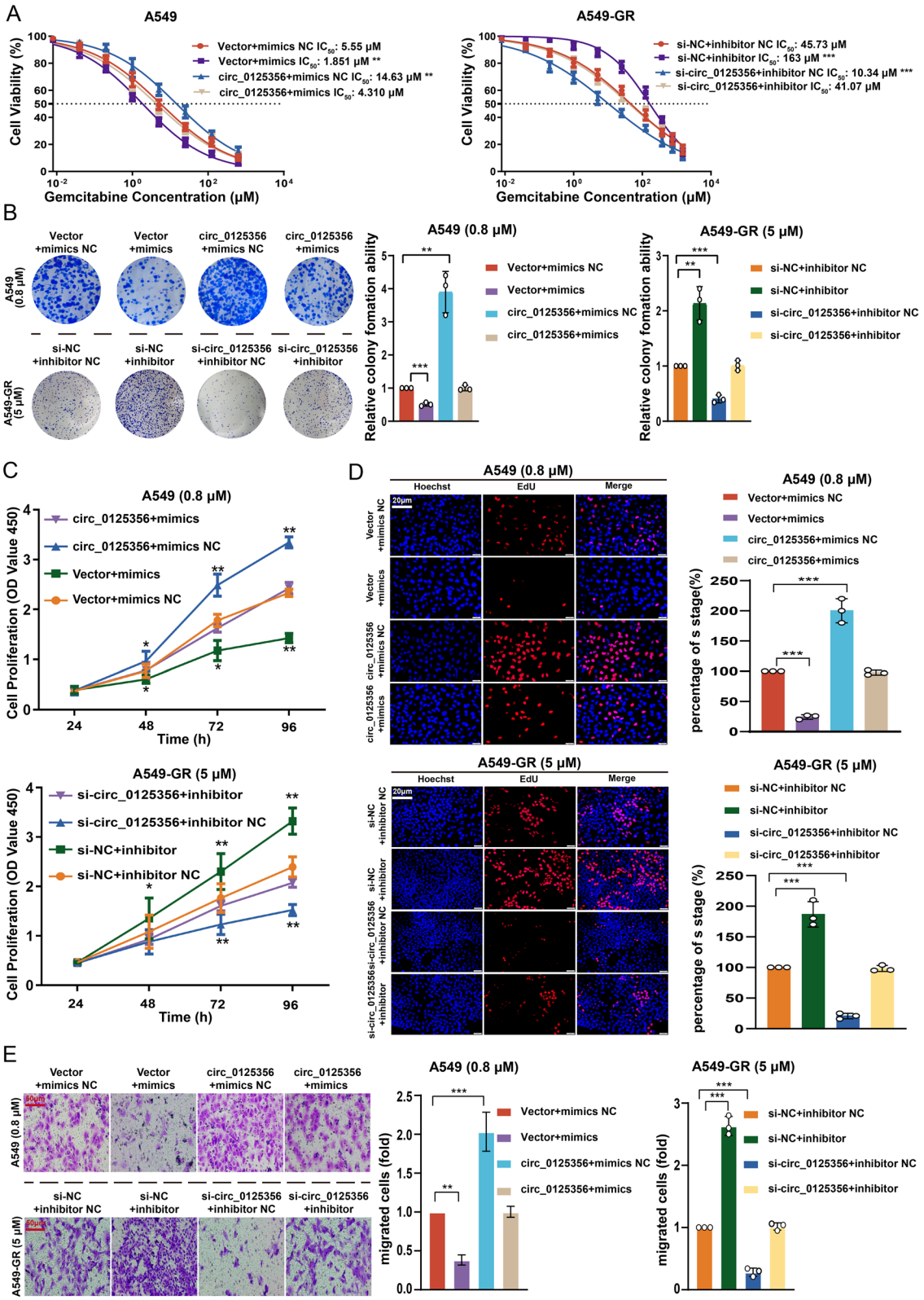

Fig. 4 (See legend on previous page.)

proliferation, migration, and drug resistance of NSCLC cells after gemcitabine treatment.

Hsa_circ_0125356 represents an effective miRNA sponge for miR-582-5p

We used three databases (Miranda, TargetScan, Circbank) to predict that 12 miRNAs could bind to hsa_circ_0125356 (Fig. 3A and Supplementary Table S7). qRT-PCR analysis further demonstrated that compared with the corresponding vector group, miR-582-5p was most significantly downregulated in the overexpressing hsa_circ_0125356 group (Fig. 3B). The expression of miR-582-5p was significantly downregulated in NSCLC tissues from 25 patients compared with the corresponding adjacent tissues (Fig. 3C). The tumors with higher hsa_circ_0125356 expression had lower expression of miR-582-5p, indicating a negative correlation between hsa_circ_0125356 and miR-582-5p in NSCLC samples (Fig. 3D). Meanwhile, low miR-582-5p expression was significantly associated with higher histologic grade (Supplementary Table S5). MiR-582-5p expression was observably lower in gemcitabine-resistant A549 GR cells than in parental A549 cells (Fig. 3E). FISH analysis showed that hsa_circ_0125356 and miR-582-5p were colocalized in the cytoplasm (Fig. 3F). RIP experiments were performed in A549 and A549-GR cells and the results illustrated that hsa_circ_0125356 and miR-582-5p were significantly enriched, as they were pulled down by the anti-AGO2 antibody (Fig. 3G). The luciferase activity of cells co-transfected with hsa_circ_0125356-WT was significantly inhibited by miR-582-5p mimics, but there was no significant change in the luciferase activity of cells co-transfected with hsa_circ_0125356-MUT (Fig. 3H). The results of qRT-PCR further confirmed that hsa_circ_0125356 overexpression significantly reduced the expression of miR-582-5p, whereas hsa_circ_0125356 interference markedly increased miR-582-5p expression, suggesting that hsa_circ_0125356 could specifically bind to miR-582-5p (Fig. 3I). These data indicate that hsa_circ_0125356 acts as a miRNA sponge for miR-582-5p and negatively regulates miR-582-5p in both A549 and A549-GR cells.

Hsa_circ_0125356 regulates tumor progression and gemcitabine resistance in NSCLC cells via miR-582-5p

We next investigated the biological functions of miR-582-5p on gemcitabine resistance in NSCLC cells. The IC_{50} assays revealed that the miR-582-5p mimics markedly enhanced the sensitivity of A549 cells to gemcitabine and the effect was reversed by transfection of the hsa_circ_0125356 plasmid. Conversely, the miR-582-5p inhibitor decreased the susceptibility to gemcitabine compared with the inhibitor NC, which was abolished by silencing hsa_circ_0125356 in A549-GR cells (Fig. 4A). The results from colony formation assays, CCK-8 assays, and EdU assays showed that in A549 cells treated with gemcitabine, the inhibition of cell proliferation by miR-582-5p could be reversed by hsa_circ_0125356 overexpression (Fig. 4B–D). Moreover, the inhibition of miR-582-5p has been shown to confer resistance to gemcitabine in A549-GR cells, while silencing hsa_circ_0125356 can mitigate this effect (Fig. 4B–D). Likewise, the effects of miR-582-5p on cell migration were reversed by hsa_circ_0125356 in both A549 and A549-GR cells (Fig. 4E). Taken together, these results suggest that hsa_circ_0125356 promotes NSCLC progression and gemcitabine resistance via sponging miR-582-5p, ultimately leading to its oncogenic effect.

FGF9 was identified as a functional target gene of miR-582-5p and enhances gemcitabine resistance in NSCLC cells

We used the three databases (ENCORI, miRDB, and TargetScan) to predict the downstream target genes of miR-582-5p (Fig. 5A and Supplementary Table S8). Among these genes, we identified 17 candidate target genes that were detected by qRT-PCR. The results revealed significant downregulation of FGF9 mRNA expression after transfection with miR-582-5p mimics compared with mimics NC (Fig. 5B). Moreover, the expression of FGF9 showed the most dramatic difference after treatment with overexpressed or silencing hsa_circ_0125356 (Fig. 5C&D). Based on microRNA response element (MRE) analysis, miR-582-5p had

(See figure on next page.)

Fig. 5 FGF9, functions as a target gene of miR-582-5p, is positively correlated with hsa_circ_0125356 in NSCLC. **A** Potential target gene of miR-582-5p were predicted in the miRDB, ENCORI, and TargetScan databases. **B** qRT-PCR was used to detect the changes in the expression of 17 genes after transfection with miR-582-5p mimics. **C**, **D** Eight genes with obvious differences were selected, and the overexpression or knockdown hsa_circ_0125356 was transfected to detect the differences in mRNA expression. **E** Relative luciferase activities in A549 and A549-GR cells co-transfected with FGF9-WT or FGF9-MUT and the miR-582-5p mimics, inhibitor, or corresponding negative control. **F**, **G** The relative expression of FGF9 in A549 or A549-GR cells was analyzed by qRT-PCR and western blotting after the indicated transfections. **H, I** Immunohistochemistry was used to detect the expression difference in FGF9 between 25 patients with NSCLC and 25 patients with paracarcinoma. The correlation between miR-582-5p/hsa_circ_0125356 and FGF9 in NSCLC was analyzed using Pearson' s correlation analysis. Scale bar: 50 μm. Data are shown as the mean ± SD. $^{*}P < 0.05$; $^{**}P < 0.01$; $^{***}P < 0.001$; $^{****}P < 0.0001$

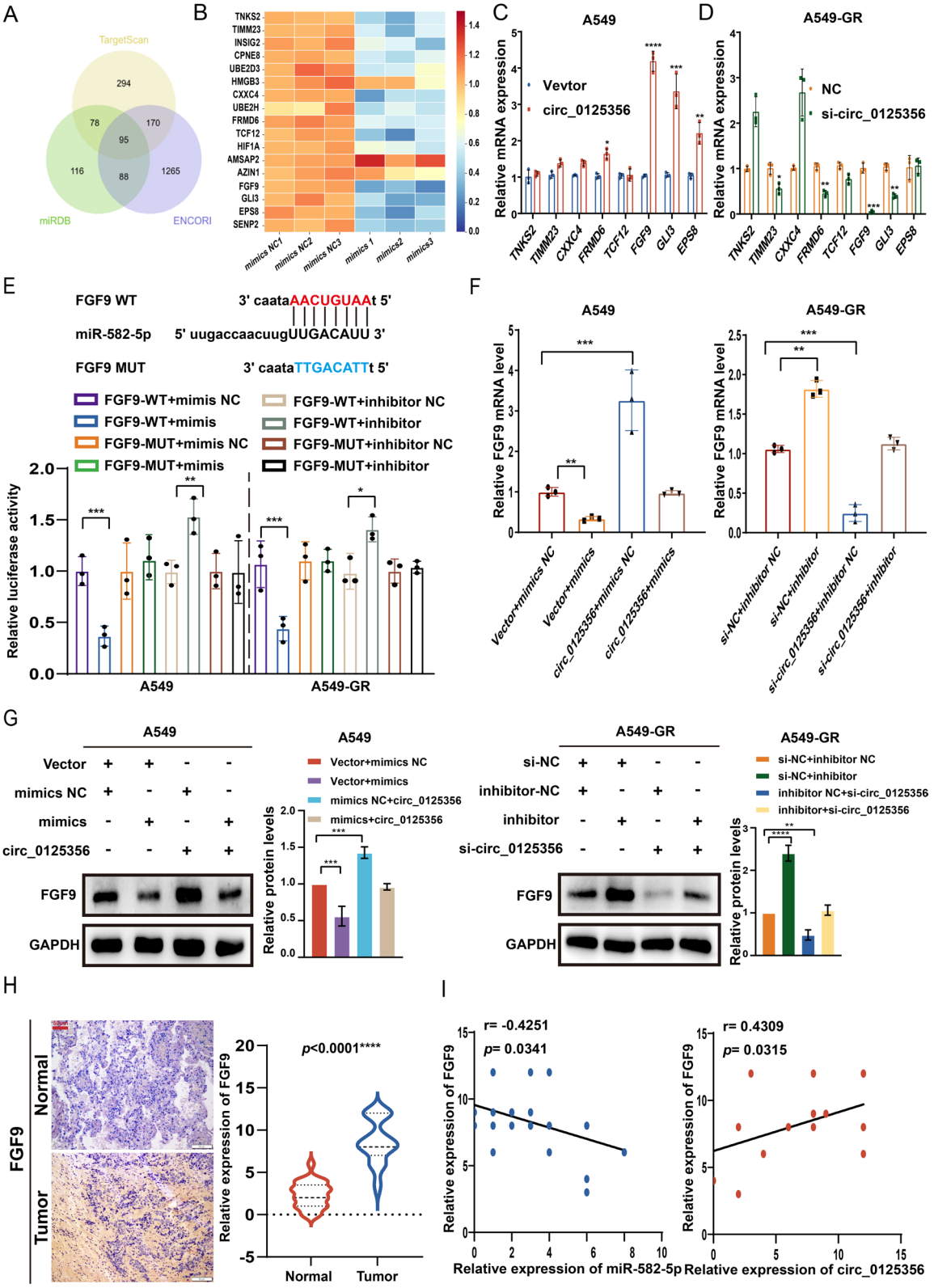

Fig. 5 (See legend on previous page.)

potential binding sites within the 3′-UTR regions of FGF9. Therefore, we inserted the wild-type (WT) and mutated (MUT) 3′-UTR of FGF9 containing each predicted binding site into luciferase reporter plasmids. The results indicated that the relative luciferase activity of A549 cells co-transfected with miR-582-5p mimics and FGF9 3′-UTR-WT was significantly decreased compared with the miR-582-5p mimics NC or FGF9 3′-UTR-MUT group. Conversely, a remarkable increase in luciferase activity was detected in A549-GR cells co-transfected with FGF9 3′-UTR-WT and miR-582-5p inhibitor, but not in the FGF9 3′-UTR-MUT group (Fig. 5E). Meanwhile, qRT-PCR and western blotting analyses confirmed that hsa_circ_0125356 overexpression enhanced the expression of FGF9, whereas miR-582-5p mimics suppressed FGF9 expression. Interestingly, the effect of miR-582-5p mimics was abolished by hsa_circ_0125356 at both the mRNA and protein (Fig. 5F&G). The cancer genome atlas (TCGA) database analysis illustrated that FGF9 expression was significantly upregulated in NSCLC tissues (Supplementary Fig. S6A). We also investigated the downstream effects of miR-582-5p on FGF9 in NSCLC tissues and adjacent tissues from 25 patients. It was found that the expression of FGF9 was markedly increased in NSCLC tissues compared with the corresponding adjacent tissues (Fig. 5H). Consistent with the cell results, NSCLC tissue samples with higher miR-582-5p expression exhibited lower FGF9 expression, indicating that FGF9 was negatively correlated with miR-582-5p and positively correlated with hsa_circ_0125356 in NSCLC samples (Fig. 5I). In addition, high FGF9 expression was significantly associated with higher histologic grade (Supplementary Table S6). In summary, FGF9 is identified as a downstream target gene of miR-582-5p and is closely related to the tumor progression of NSCLC.

Hsa_circ_0125356 maintained gemcitabine resistance through the miR-582-5p/FGF9 axis

To further investigate the effects of hsa_circ_0125356 via miR-582-5p/FGF9 axis on gemcitabine resistance, we designed RNA-seq to determine the gene set that may regulate the sensitivity of A549-GR cells. The transcriptome sequencing showed that FGF9 expression was significantly higher in A549-GR cells than in A549 cells (Fig. 6A&B). The levels of FGF9 measured with ELISAs kit were notably increased in culture supernate from NSCLC cell lines compared with the cell free culture media, especially in the supernatant of gemcitabine-resistant A549 GR cells (Fig. 6C). In addition, the results of western blot showed that the expression of FGFR3 was higher in A549-GR cells than in A549 cells or other NSCLC cells (Supplementary Fig. S6B). Next, we transfected overexpressed Flag-FGF9 plasmids (OE-FGF9) and FGF9-specific shRNAs (shFGF9) into A549 and A549-GR cells. The results of qRT-PCR and western blotting revealed that shFGF9#3 significantly reduced FGF9 expression compared with scrambled shRNA, while Flag-FGF9 markedly upregulated FGF9 expression compared with vector plasmids (Supplementary Fig. S7A-D). The values of IC_{50} were significantly reduced after FGF9 knockdown in A549-GR cells under gemcitabine exposure, but markedly increased after FGF9 overexpression in A549 cells, suggesting that the knockdown of FGF9 promoted the tumor cells more sensitive to gemcitabine, while FGF9 overexpression obviously increased gemcitabine resistance (Fig. 6D). Similar results were obtained by cell viability assay, colony formation assay, and migration ability assay (Fig. 6E–G). Furthermore, it was reported that FGF9 can provide cells with strong repairability to fight DNA damage [25, 26]. Thus, we stimulated the cells with gemcitabine for 24 or 48 h to cause the accumulation of DNA damage. The

(See figure on next page.)

Fig. 6 Hsa_circ_0125356 regulated gemcitabine resistance through sponging the miR-582-5p/FGF9 axis. **A–B** Transcriptome sequencing analysis of A549 and A549-GR cells. **C** The expression of FGF9 in the culture medium of NSCLC and A549-GR cells was detected by ELISAs kit. **D** The sensitivity to gemcitabine in stably transfected A549 and A549-GR cells treated with gemcitabine was investigated via CCK-8 assays (IC_{50}). **E–G** CCK-8 assays (cell viability), colony formation assays, and Transwell assays were used to detect the changes in proliferation and migration of stably transfected A549 and A549-GR cells treated with gemcitabine. Scale bar: 50 μm. **H** Confocal microscopy was used to analyze the effect of FGF9 on the distribution of γH2AX foci after gemcitabine treatment. Scale bar: 20 μm. **I** Apoptosis (flow cytometry) of A549 and A549-GR cells transfected with knockdown or overexpression of FGF9 after gemcitabine treatment. **J–M** A549 and A549-GR cells were transfected with miR-582-5p mimics and miR-582-5p inhibitor or overexpression and knockdown of hsa_circ_0125356 and FGF9. The proliferative ability of the indicated cells treated with gemcitabine was investigated via CCK-8 assays (IC_{50} and cell viability), colony formation, and EdU assays. Scale bar: 20 μm. **N** Transwell assays were used to detect the changes in the migration of miR-582-5p mimics and miR-582-5p inhibitors or the overexpression and knockdown of hsa_circ_0125356 and FGF9-transfected A549 and A549-GR cells treated with gemcitabine. Scale bar: 50 μm. Data are shown as the mean ± SD. $^{*}P < 0.05$; $^{**}P < 0.01$; $^{***}P < 0.001$; $^{****}P < 0.0001$

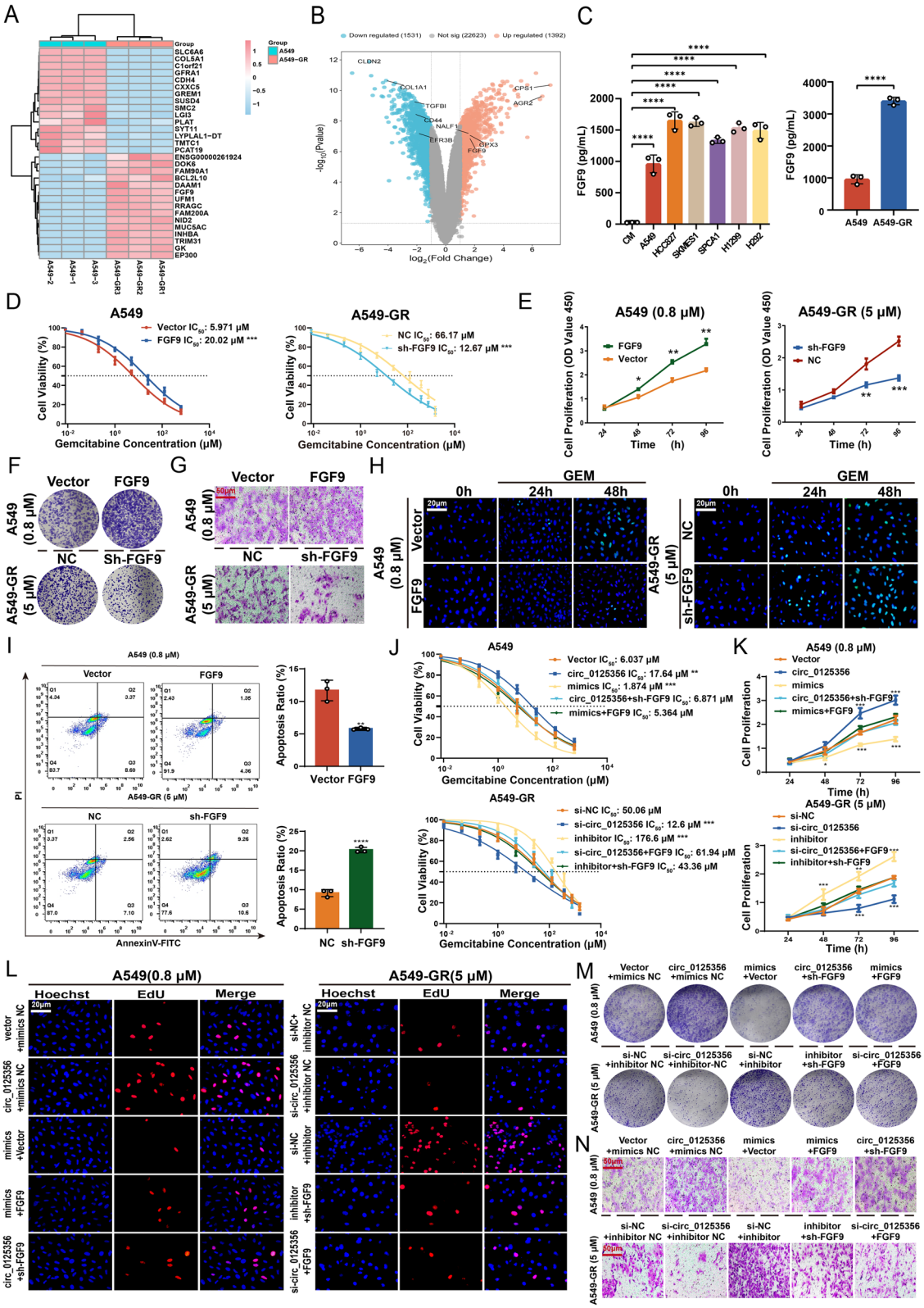

Fig. 6 (See legend on previous page.)

immunofluorescence results showed that the knockdown of FGF9 enhanced the expression of γH2AX, a DNA damage marker, in gemcitabine-resistant cell lines under gemcitabine loading. The opposite result was observed in gemcitabine-resistant cell lines overexpressing FGF9 (Fig. 6H). Flow cytometry showed that overexpressed FGF9 significantly decreased apoptosis in A549 cells, while silencing FGF9 increased susceptibility to apoptosis in A549-GR cells under gemcitabine exposure (Fig. 6I). Additionally, a series of rescue experiments were performed to further explore whether hsa_circ_0125356 promotes gemcitabine resistance by sponging the miR-582-5p/FGF9 pathway in NSCLC cells. The results showed that overexpressing FGF9 strongly abolished the inhibitory effects induced by hsa_circ_0125356 knockdown and miR-582-5p overexpression, whereas silencing FGF9 led to the opposite results (Fig. 6J–N). These findings revealed that hsa_circ_0125356 promoted gemcitabine resistance by sponging the miR-582-5p/FGF9 pathway.

FGF9 enhances gemcitabine resistance through the canonical and noncanonical WNT signaling pathways

Previous studies have shown that FGF9 is associated with tumor progression and drug resistance by regulating the WNT and mitogen-activated protein kinase (MAPK) signaling pathways [27, 28]. Kyoto Encyclopedia of Genes and Genomes (KEGG) pathway analysis revealed a significant enrichment of genes linked to the WNT and MAPK pathway in A549-GR cells (Fig. 7A). However, gene set enrichment analysis (GSEA) suggested that the key genes controlling WNT signaling pathway were more dominant than MAPK signaling pathway. (Fig. 7B). Therefore, we speculated that FGF9 maintains gemcitabine resistance in NSCLC cells mainly via the WNT signaling pathway. Western blot analysis demonstrated that overexpression of FGF9 reversed the changes in canonical WNT signaling pathway-related proteins (GSK-3β phosphorylation, ERK1/2 phosphorylation, and β-catenin phosphorylation), noncanonical WNT signaling pathway-related proteins (Daam1, RhoA, and ROCK2), and apoptosis-related proteins caused by knockdown of hsa_circ_0125356 in gemcitabine-resistant A549-GR cells after gemcitabine treatment, whereas silencing FGF9 restored the changes in corresponding protein caused by hsa_circ_0125356 overexpression in parental A549 cells (Fig. 7C–H). WAY 316606 and XAV-939 were two small molecules antagonists that inhibited activation of the WNT signaling pathway [29, 30]. In this study, we found that WAY 316606 or XAV-939 abolished the changes in the IC_{50} values and formed colonies induced by hsa_circ_0125356 overexpression in parental A549 cells after gemcitabine treatment. In addition, WAY 316606 or XAV-939 treatment further enhanced the inhibitory effect on the IC_{50} values and formed colonies caused by hsa_circ_0125356 knockdown in A549-GR cells, indicating that WAY 316606 and XAV-939 could reverse gemcitabine resistance induced by hsa_circ_0125356 in NSCLC cells (Fig. 7I-K). Moreover, the overexpression of hsa_circ_0125356 remarkably enhanced the expression of β-catenin in parental A549 cells, whereas silencing hsa_circ_0125356 significantly inhibited the expression of β-catenin in A549-GR cells. These effects on β-catenin expression induced by hsa_circ_0125356 could be reversed by WAY 316606 and XAV-939 treatment (Fig. 7L). Interestingly, the changes in ROCK2 expression caused by hsa_circ_0125356 overexpression or hsa_circ_0125356 knockdown were abolished after treatment with WAY 316606 (an inhibitor of WNT total signaling pathway), but not with XAV-939 (an inhibitor of WNT canonical signaling pathway), suggesting that both canonical and noncanonical WNT signaling pathways were involved in the gemcitabine resistance induced by hsa_circ_0125356 (Fig. 7L). These results collectively demonstrated that hsa_circ_0125356 regulated the expression of FGF9 to maintain gemcitabine resistance via the WNT canonical and non-canonical signaling pathways.

(See figure on next page.)

Fig. 7 FGF9 enhances gemcitabine resistance by promoting the WNT canonical and noncanonical signaling pathways. **A** Genomes (KEGG) analysis based on RNA-seq data. **B** GSEA enrichment analysis of signaling pathways. **C-F** Western blotting analysis was performed to assess the levels of WNT signaling pathway-related proteins (GSK-3β phosphorylation, ERK1/2 phosphorylation, and β-catenin phosphorylation) and noncanonical WNT signaling pathway-related proteins (Daam1, RhoA, and ROCK2) in A549 and A549-GR cells from different groups treated with gemcitabine. GAPDH was used as a loading control. **G**, **H** Western blotting analysis was performed to assess the levels of apoptosis-related proteins in A549 and A549-GR cells from different groups treated with gemcitabine. β-Actin was used as a loading control. **I-K** A549 and A549-GR cells transfected with overexpressed hsa_circ_0125356, knockdown of hsa_circ_0125356, WAY 316606, and XAV-939, and the proliferative ability of the indicated cells treated with gemcitabine was investigated via CCK-8 assays (IC_{50}) and colony formation assays. **L** Western blotting was performed to assess the protein levels of β-catenin and ROCK2 in A549 and A549-GR cells treated with gemcitabine after transfected with overexpression hsa_circ_0125356, knockdown of hsa_circ_0125356, WAY 316606, and XAV-939. Data are shown as the mean ± SD. $^{*}P < 0.05$; $^{**}P < 0.01$; $^{***}P < 0.001$; $^{****}P < 0.0001$ between the indicated groups

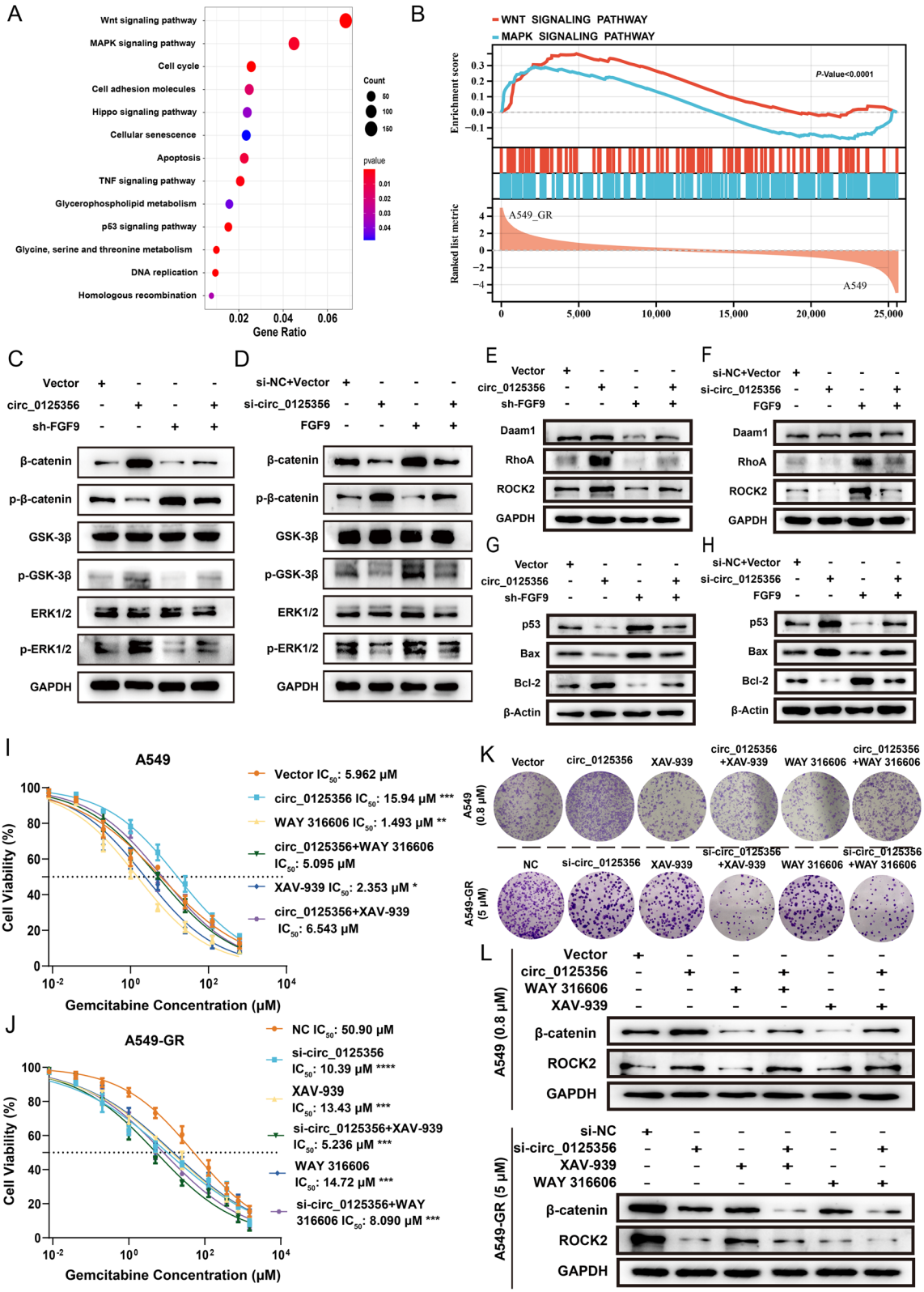

Fig. 7 (See legend on previous page.)

Hsa_circ_0125356 promoted gemcitabine resistance in NSCLC via the WNT canonical and non-canonical signaling pathways in vivo

A mouse xenograft tumor model was constructed to determine the effect of hsa_circ_0125356 on gemcitabine resistance in vivo (Fig. 8A). In the absence of gemcitabine, subcutaneous transplantation of hsa_circ_0125356-overexpressing A549 cells or hsa_circ_0125356-silenced A549-GR cells barely affected tumor growth compared with the NC group, however, the transplantation of hsa_circ_0125356-silenced A549-GR cells significantly reduced tumor size, volume, and weight after gemcitabine treatment, indicating that the silence of hsa_circ_0125356 enhanced the sensitivity of tumor cells to gemcitabine, whereas hsa_circ_0125356-overexpressing A549 cells displayed the opposite effects (Fig. 8B–E). TUNEL apoptosis assays revealed a significant decrease in the percentage of apoptosis-positive cells in the hsa_circ_0125356 overexpressing group and an increase in the hsa_circ_0125356 silenced group (Fig. 8F and G). Moreover, Ki-67 staining indicated that hsa_circ_0125356 overexpression significantly increased the percentage of Ki-67-positive cells under gemcitabine treatment compared with the NC group, whereas silencing hsa_circ_0125356 led to the opposite results (Fig. 8H and I).

Immunohistochemical analyses revealed that the expression of FGF9 was significantly reduced in the hsa_circ_0125356 knockdown group treated with gemcitabine, whereas the opposite result was observed in the hsa_circ_0125356 overexpression group (Fig. 9A and B). In addition, the FISH results showed that knockdown of hsa_circ_0125356 significantly increased the expression of miR-582-5p after gemcitabine treatment, whereas overexpression of hsa_circ_0125356 reduced the expression of miR-582-5p (Fig. 9C and D). Consistent with the results in vitro, the overexpression of hsa_circ_0125356 notably activated the expression of canonical and noncanonical WNT pathway-related proteins, and apoptosis-related protein, whereas knockdown of hsa_circ_0125356 exhibited a oppsite effect (Fig. 9E–G). These results indicated that hsa_circ_0125356 regulated the miR-582-5p/FGF9 axis to enhance gemcitabine resistance in NSCLC via the WNT canonical and non-canonical signaling pathways in vivo.

Discussion

NSCLC is one of the most common malignancies and the leading cause of lung cancer-related death [31]. In recent years, the prognosis of patients with NSCLC has improved considerably with the application of molecular targeted therapy, immunotherapy, and radiotherapy, as well as the development of new chemotherapeutic drugs [32, 33]. However, most patients with NSCLC develop acquired drug resistance after months of gemcitabine treatment, eventually leading to a 5-year overall survival rate of less than 20% [34, 35]. Therefore, there is an urgent need to identify mechanisms related to gemcitabine resistance and develop new therapeutic strategies to improve the survival outcomes of patients with NSCLC.

Recently, circRNAs have been proven to play crucial roles in drug resistance in malignant tumors, including NSCLC. For instance, studies have demonstrated that circPSMC3 restores sensitivity to gefitinib by regulating the miR-10a-5p/PTEN axis [36]. Moreover, circ_0004015 has been shown to regulate PDPK1 expression to maintain gefitinib resistance in miR-1183 sponges [37]. However, the specific functions of circRNAs and their novel mechanism of gemcitabine resistance in NSCLC continue to offer fertile ground for exploration and investigation.

Here, a gemcitabine-resistant NSCLC cell model (A549-GR) was constructed and the IC_{50} of A549-GR cells increased by nearly 19.3 times compared with that of wild-type NSCLC cells (A549). Next, using circRNA sequencing technology, we identified a novel hsa_circ_0125356 as being among some of the circRNAs with the largest expression differences between gemcitabine-resistant and parental cells. The database (Circbase) analysis showed that hsa_circ_0125356 was generated by chromosome chr4 (q28.3) on human SLC7A11 gene exon reverse splicing. Then, a series of experiments were performed to verify that hsa_circ_0125356 exhibited a circular structure with high

(See figure on next page.)

Fig. 8 Knockdown or overexpression of hsa_circ_0125356 affected gemcitabine sensitivity in vivo. **A** An outline of the tumor inoculation and systemic injection process. **B** BALB/c nude mice were subcutaneously injected with stably transfected A549 cells. Images of gross tumors dissected from the subcutaneous xenograft model and weight of resected tumor in the xenograft model. **C** Tumor volumes were recorded twice a week. **D** BALB/c nude mice were subcutaneously injected with stably transfected A549-GR cells. Images of gross tumors dissected from the subcutaneous xenograft model and weight of resected tumor in the xenograft model. **E** Tumor volumes were recorded twice a week. **F**, **G** TUNEL assay was used to detect changes in apoptosis from the subcutaneous xenograft model. Scale bar: 20 μm. **H, I** Representative images of IHC for Ki-67 in xenografts. Scale bar: 20 μm and 50 μm. Data are shown as the mean ± SD. $^{*}P < 0.05$; $^{**}P < 0.01$; $^{***}P < 0.001$; $^{****}P < 0.0001$

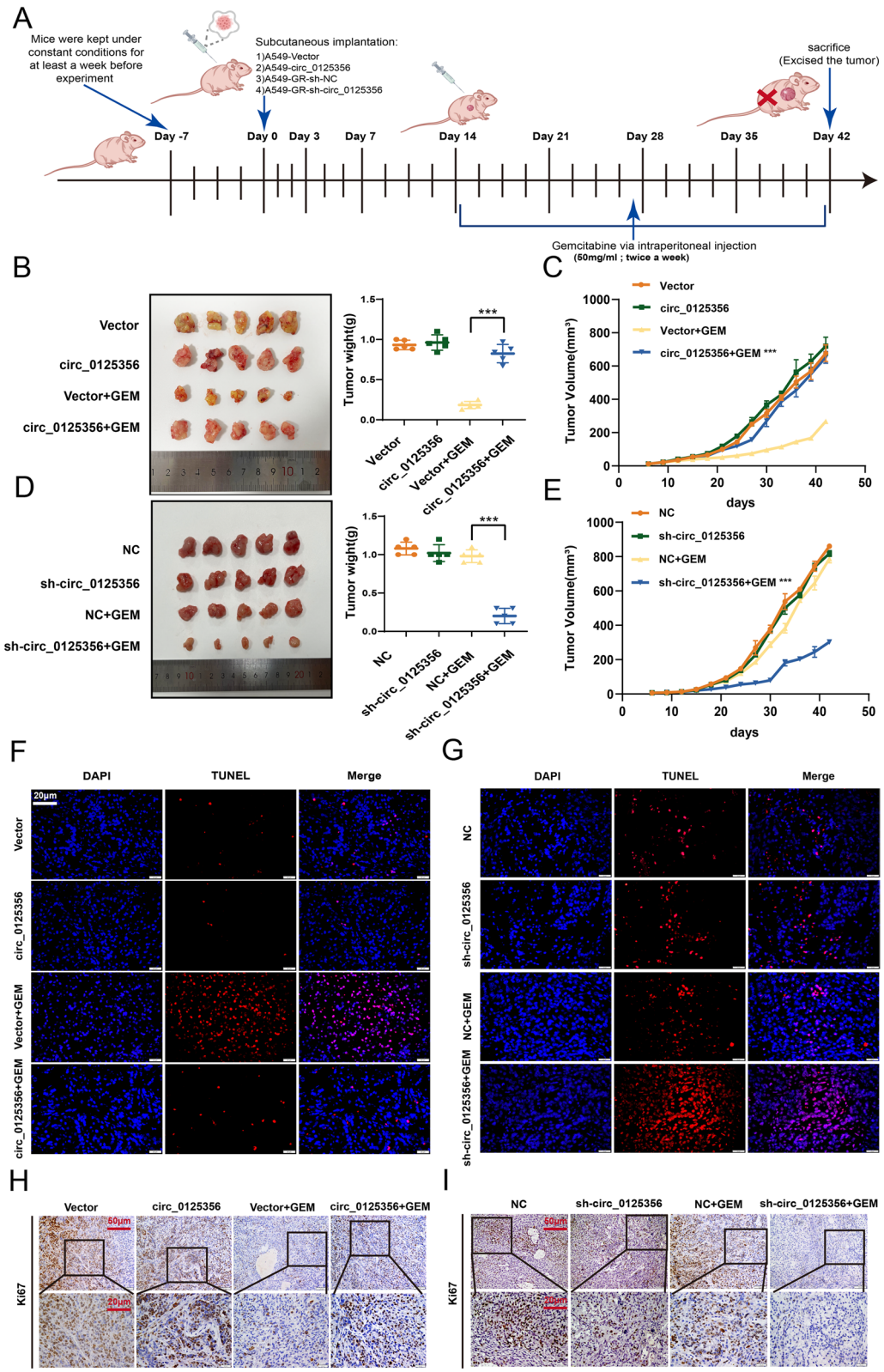

Fig. 8 (See legend on previous page.)

stability and was localized in the cytoplasm. Intriguingly, our results revealed that hsa_circ_0125356 was upregulated in tumor tissues from NSCLC patients and correlated with poorer prognosis. In addition, the resistance-related functional assays demonstrated that hsa_circ_0125356 promoted gemcitabine resistance in NSCLC cells. Subcutaneous transplantation of hsa_circ_0125356-silenced A549-GR cells significantly enhanced the sensitivity of cells to gemcitabine in tumor-bearing nude mice, indicating that hsa_circ_0125356 may be involved in gemcitabine resistance in NSCLC.

Increasing evidence has revealed that circRNAs regulate miRNAs by competitively binding to target sites on protein-encoding mRNA molecules [38–40]. MiR-582-5p was selected as the candidate target miRNA of hsa_circ_0125356 using bioinformatics tools (Miranda, TargetScan, and Circbank). The results of FISH experiments demonstrated the localization of hsa_circ_0125356 and miR-582-5p in the cytoplasm. The RIP assays and double-luciferase reporter experiment further confirmed that hsa_circ_0125356 could act as a ceRNA for miR-582-5p. Interestingly, statistical analysis of clinical samples revealed that miR-582-5p expression was significantly decreased in NSCLC. Combined analysis of qRT-PCR and clinical samples showed a negative correlation between the expression of hsa_circ_0125356 and miR-582-5p in NSCLC tissues. Previous research has indicated that miR-582-5p acts as a tumor suppressor in the development of gastric cancer, breast cancer, and NSCLC [41–44]. However, it is needed to confirm whether miR-582-5p is involved in gemcitabine resistance in NSCLC. Cell function experiments in our study showed that the interaction between hsa_circ_0125356 and miR-582-5p is a novel strategy for reversing gemcitabine resistance in NSCLC. The in vitro rescue experiments also confirmed that miR-582-5p could suppress tumor progression and gemcitabine resistance induced by hsa_circ_0125356 in NSCLC.

FGF9 is involved in serial types of cancer, and abnormal activation of FGF9 signaling is associated with tumor progression in NSCLC. FGF9 expression is upregulated in NSCLC and represents an unfavorable prognostic indicator for patients [45–47]. However, the specific role of FGF9 in gemcitabine resistance in NSCLC remains unknown. In this study, we predicted FGF9 as a potential downstream target gene of miR-582-5p through bioinformatics analysis. Dual-luciferase reporter gene assay and western blotting confirmed that FGF9 was the downstream target of miR-582-5p. Combined analysis of clinical samples and the TCGA database confirmed that FGF9 expression was significantly elevated in NSCLC. Meanwhile, hsa_circ_0125356 overexpression enhanced the expression of FGF9, whereas miR-582-5p mimics suppressed FGF9 expression, suggesting an obvious regulatory relationship between them. Based on the clinical samples and bioinformatics analysis results, we speculated that FGF9 may mediate gemcitabine resistance in NSCLC and affect its proliferation and migration. As expected, this study revealed that hsa_circ_0125356 promoted tumor progression and gemcitabine resistance by sponging the miR-582-5p/FGF9 pathway.

FGF9 has recently been shown to induce cell proliferation, migration, and chemotherapy resistance in lung cancer cells by regulating the WNT and MAPK signaling pathways [48–50]. The WNT signaling pathway is an important molecular signaling pathway in tumor cells and is significantly correlated with tumor initiation, metastasis, recurrence, and drug resistance [51–53]. It has been reported that activation of noncanonical WNT signaling regulates enzalutamide sensitivity in prostate cancer [54]. Moreover, OTULIN-mediated WNT/β-catenin activation upon genotoxic treatment promotes drug resistance and metastasis in breast cancer [55]. Our results demonstrated that hsa_circ_0125356 could enhance gemcitabine resistance in NSCLC by regulating the WNT canonical and non-canonical signaling pathways in vitro and in vivo, thereby promoting DNA damage repair and inhibiting apoptosis. In addition, WAY 316606 and XAV-939 are inhibitors of the WNT signaling pathway and can reverse the effects induced by hsa_circ_0125356. These results provide convinced evidence that hsa_circ_0125356 is involved in gemcitabine resistance in

(See figure on next page.)

Fig. 9 Hsa_circ_0125356 activates the WNT canonical and non-canonical signaling pathways by regulating the miR-582-5p/FGF9 axis to maintain gemcitabine resistance in vivo. **A**, **B** Representative images of FGF9 IHC in xenografts. Scale bar: 20 μm and 50 μm. **C**, **D** Representative images of FISH analyses of hsa_circ_0125356 and miR-582-5p in xenografts. Scale bar: 20 μm. **E** Western blotting analysis was performed to assess the protein levels of the WNT canonical signaling pathways (ERK1/2, p-ERK1/2, β-catenin, p-β-catenin, GSK-3β, p-GSK-3β) in xenografts from different treatments. GAPDH was used as a loading control. **F** Western blotting was performed to assess the protein levels of the WNT non-canonical signaling pathways (Daam1, RhoA, and ROCK2) in xenografts from different treatments. GAPDH was used as a loading control. **G** Western blotting was performed to assess the levels of apoptosis-related proteins in xenografts from different treatments. β-Actin was used as a loading control. Data are shown as the mean ± SD. $^{*}P < 0.05$; $^{**}P < 0.01$; $^{***}P < 0.001$; $^{****}P < 0.0001$

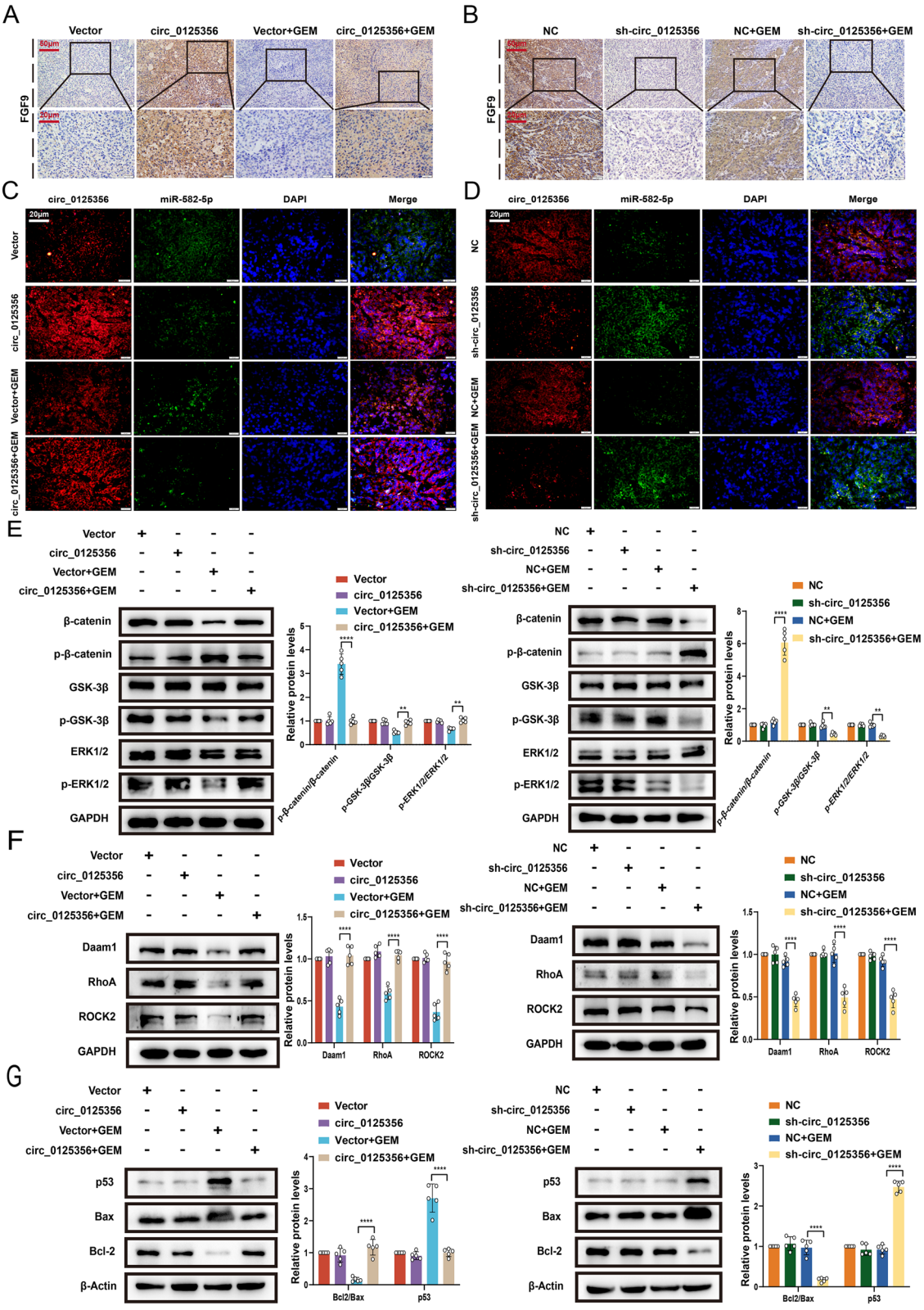

Fig. 9 (See legend on previous page.)

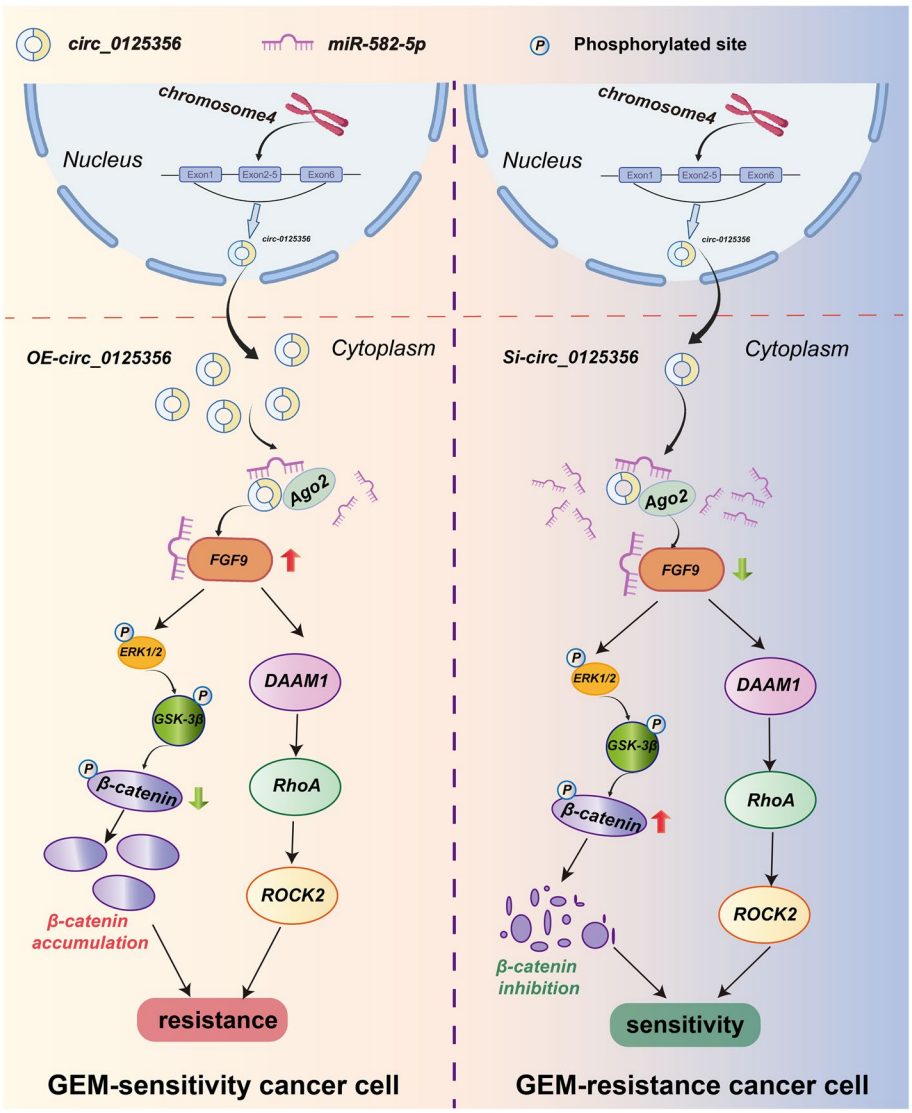

Fig. 10 Schematic illustration of the mechanism by which hsa_circ_0125356/miR-582-5p/FGF9 axis activates the WNT canonical and non-canonical signaling pathway and promotes gemcitabine-resistance in NSCLC

NSCLC through the WNT canonical and non-canonical signaling pathways.

In conclusion, for the first time, we revealed that hsa_circ_0125356 was significantly upregulated and served as a biomarker of gemcitabine resistance in NSCLC by sponging the miR-582-5p/FGF9 axis to regulate the WNT canonical and non-canonical signaling pathways (Fig. 10). Understanding the hsa_circ_0125356/ miR-582-5p/FGF9/WNT axis could provide a new direction for the identification of therapeutic targets for gemcitabine-resistant NSCLC.

Abbreviations

ActD	Actinomycin D
BCa	Bladder cancer
circRNAs	Circular RNAs
CISH	Chromogenic in situ hybridization
EdU	5-Ethynyl-2′-deoxyuridine
FISH	Fluorescence in situ hybridization
FGF9	Fibroblast growth factor 9
GEM	Gemcitabine
IHC	Immunohistochemistry
ISH	In situ hybridization
MRE	MicroRNA response element
NSCLC	Non-small cell lung cancer
ncRNA	Non-coding RNA
OE-FGF9	Overexpressed Flag-FGF9 plasmids
PABPC1	Poly(A)-binding protein cytoplasmic 1

PVDF	Polyvinylidene difluoride
QRT-PCR	Quantitative real-time PCR
RIP	RNA immunoprecipitation
RBP	RNA-binding protein
shFGF9	FGF9-specific shRNAs
TCGA	The cancer genome atlas

Supplementary Information

The online version contains supplementary material available at https://doi.org/10.1186/s12943-025-02259-0.

Supplementary Material 1.

Supplementary Material 2.

Acknowledgements
We thank the First People's Hospital of Jiujiang for kindly providing the NSCLC tissue samples.

Authors' contributions
C. and F. participated in research design. X., W., H., Q.and P. conducted the experiments. X., W., C. and N. performed data analysis. X., C. and F. wrote or contributed to the writing of the manuscript. All authors read and approve the final manuscript.

Funding
This study was supported by the National Natural Science Foundation of China (No. 82160708, 81760672 and 82260717).

Data availability
No datasets were generated or analysed during the current study.

Declarations

Consent for publication
All authors agreed to the publication of the manuscript.

Competing interests
The authors declare no competing interests.

Author details
[1]School of Pharmacy, Jiangxi Medical College, Nanchang University, Nanchang 330006, P. R. China. [2]Key Laboratory of New Drug Transformation and Evaluation of Jiangxi Province, Nanchang 330031, P. R. China.

Received: 2 October 2024 Accepted: 4 February 2025
Published online: 27 February 2025

References

1. Ferlay J, Colombet M, Soerjomataram I, Mathers C, Parkin DM, Piñeros M, Znaor A, Bray F. Estimating the global cancer incidence and mortality in 2018: GLOBOCAN sources and methods. Int J Cancer. 2019;144:1941–53.
2. Del VV, Denti MA. microRNA and Lung Cancer. Adv Exp Med Biol. 2015;889:153–77.
3. Seidl C, Panzitt K, Bertsch A, Brcic L, Schein S, Mack M, Leithner K, Prinz F, Olschewski H, Kornmueller K, Hrzenjak A. MicroRNA-182-5p regulates hedgehog signaling pathway and chemosensitivity of cisplatin-resistant lung adenocarcinoma cells via targeting GLI2. Cancer Lett. 2020;469:266–76.
4. Zhong L, Sun S, Shi J, Cao F, Han X, Chen Z. MicroRNA-125a-5p plays a role as a tumor suppressor in lung carcinoma cells by directly targeting STAT3. Tumour Biol. 2017;39:1393392085.
5. Dutta RK, Chinnapaiyan S, Unwalla H. Aberrant MicroRNAomics in Pulmonary Complications: Implications in Lung Health and Diseases. Mol Ther Nucleic Acids. 2019;18:413–31.
6. Chen L, Huang C, Wang X, Shan G. Circular RNAs in Eukaryotic Cells. Curr Genomics. 2015;16:312–8.
7. Pandit B, Royzen M. Recent Development of Prodrugs of Gemcitabine. Genes (Basel). 2022;13(3):466.
8. Jiang H, Zheng Y, Qian J, Mao C, Xu X, Li N, Xiao C, Wang H, Teng L, Zhou H, et al. Efficacy and safety of sintilimab in combination with chemotherapy in previously untreated advanced or metastatic nonsquamous or squamous NSCLC: two cohorts of an open-label, phase 1b study. Cancer Immunol Immunother. 2021;70:857–68.
9. Boukovinas I, Souglakos J, Hatzidaki D, Kakolyris S, Ziras N, Vamvakas L, Polyzos A, Geroyianni A, Agelidou A, Agelaki S, et al. Docetaxel plus gemcitabine as front-line chemotherapy in elderly patients with lung adenocarcinomas: a multicenter phase II study. Lung Cancer. 2009;63:77–82.
10. Georgoulias V, Papadakis E, Alexopoulos A, Tsiafaki X, Rapti A, Veslemes M, Palamidas P, Vlachonikolis I. Platinum-based and non-platinum-based chemotherapy in advanced non-small-cell lung cancer: a randomised multicentre trial. Lancet. 2001;357:1478–84.
11. Mini E, Nobili S, Caciagli B, Landini I, Mazzei T. Cellular pharmacology of gemcitabine. Ann Oncol. 2006;17(Suppl 5):v7–12.
12. Huang P, Chubb S, Hertel LW, Grindey GB, Plunkett W. Action of 2',2'-difluorodeoxycytidine on DNA synthesis. Cancer Res. 1991;51:6110–7.
13. Nordh S, Ansari D, Andersson R. hENT1 expression is predictive of gemcitabine outcome in pancreatic cancer: a systematic review. World J Gastroenterol. 2014;20:8482–90.
14. Huang G, Li S, Yang N, Zou Y, Zheng D, Xiao T. Recent progress in circular RNAs in human cancers. Cancer Lett. 2017;404:8–18.
15. Zhang Y, Zhang XO, Chen T, Xiang JF, Yin QF, Xing YH, Zhu S, Yang L, Chen LL. Circular intronic long noncoding RNAs. Mol Cell. 2013;51:792–806.
16. Li Z, Huang C, Bao C, Chen L, Lin M, Wang X, Zhong G, Yu B, Hu W, Dai L, et al. Exon-intron circular RNAs regulate transcription in the nucleus. Nat Struct Mol Biol. 2015;22:256–64.
17. Lasda E, Parker R. Circular RNAs: diversity of form and function. RNA. 2014;20:1829–42.
18. Zhang L, Zhou Q, Qiu Q, Hou L, Wu M, Li J, Li X, Lu B, Cheng X, Liu P, et al. CircPLEKHM3 acts as a tumor suppressor through regulation of the miR-9/BRCA1/DNAJB6/KLF4/AKT1 axis in ovarian cancer. Mol Cancer. 2019;18:144.
19. Li Z, Ruan Y, Zhang H, Shen Y, Li T, Xiao B. Tumor-suppressive circular RNAs: Mechanisms underlying their suppression of tumor occurrence and use as therapeutic targets. Cancer Sci. 2019;110:3630–8.
20. Yu H, Chen Y, Jiang P. Circular RNA HIPK3 exerts oncogenic properties through suppression of miR-124 in lung cancer. Biochem Biophys Res Commun. 2018;506:455–62.
21. Yao Y, Hua Q, Zhou Y. CircRNA has_circ_0006427 suppresses the progression of lung adenocarcinoma by regulating miR-6783-3p/DKK1 axis and inactivating Wnt/β-catenin signaling pathway. Biochem Biophys Res Commun. 2019;508:37–45.
22. Yan L, Liu G, Cao H, Zhang H, Shao F. Hsa_circ_0035483 sponges hsa-miR-335 to promote the gemcitabine-resistance of human renal cancer cells by autophagy regulation. Biochem Biophys Res Commun. 2019;519:172–8.
23. Huang W, Lu Y, Wang F, Huang X, Yu Z. Circular RNA circRNA_103809 Accelerates Bladder Cancer Progression and Enhances Chemo-Resistance by Activation of miR-516a-5p/FBXL18 Axis. Cancer Manag Res. 2020;12:7561–8.
24. Vo JN, Cieslik M, Zhang Y, Shukla S, Xiao L, Zhang Y, Wu YM, Dhanasekaran SM, Engelke CG, Cao X, et al. The Landscape of Circular RNA in Cancer. Cell. 2019;176:869–81.
25. Li A, Li XM, Song CG, Xiao X, Yao WM, Tian HS. Fibroblast growth factor 9 attenuates sepsis-induced fulminant hepatitis in mice. Amino Acids. 2022;54:1069–81.
26. Chang CC, Takada YK, Cheng CW, Maekawa Y, Mori S, Takada Y. FGF9, a potent mitogen, is a new ligand for integrin αvβ3, and the FGF9 mutant defective in integrin binding acts as an antagonist. Cells. 2024;13:307–20.
27. Yang F, Whelan EC, Guan X, Deng B, Wang S, Sun J, Avarbock MR, Wu X, Brinster RL. FGF9 promotes mouse spermatogonial stem cell proliferation mediated by p38 MAPK signalling. Cell Prolif. 2021;54: e12933.
28. Sun Y, Ying X, Li R, Weng M, Shi J, Chen Z. FGF9 Promotes Expression of HAS2 in Palatal Elevation via the Wnt/β-Catenin/TCF7L2 Pathway. Biomolecules. 2022;12(11):1639.

29. Moore WJ, Kern JC, Bhat R, Commons TJ, Fukayama S, Goljer I, Krishnamurthy G, Magolda RL, Nogle L, Pitts K, et al. Modulation of Wnt signaling through inhibition of secreted frizzled-related protein I (sFRP-1) with N-substituted piperidinyl diphenylsulfonyl sulfonamides. J Med Chem. 2009;52:105–16.
30. Huang SM, Mishina YM, Liu S, Cheung A, Stegmeier F, Michaud GA, Charlat O, Wiellette E, Zhang Y, Wiessner S, et al. Tankyrase inhibition stabilizes axin and antagonizes Wnt signalling. Nature. 2009;461:614–20.
31. Sui J, Yang S, Liu T, Wu W, Xu S, Yin L, Pu Y, Zhang X, Zhang Y, Shen B, Liang G. Molecular characterization of lung adenocarcinoma: A potential four-long noncoding RNA prognostic signature. J Cell Biochem. 2019;120:705–14.
32. Thai AA, Solomon BJ, Sequist LV, Gainor JF, Heist RS. Lung cancer. Lancet. 2021;398:535–54.
33. Rotow J, Bivona TG. Understanding and targeting resistance mechanisms in NSCLC. Nat Rev Cancer. 2017;17:637–58.
34. Zhou J, Kang Y, Chen L, Wang H, Liu J, Zeng S, Yu L. The Drug-Resistance Mechanisms of Five Platinum-Based Antitumor Agents. Front Pharmacol. 2020;11:343.
35. Wang YZ, An Y, Li BQ, Lu J, Guo JC. Research progress on circularRNAs in pancreatic cancer: emerging but promising. Cancer Biol Ther. 2019;20:1163–71.
36. Zhu H, Du F, Cao C. Restoration of circPSMC3 sensitizes gefitinib-resistant esophageal squamous cell carcinoma cells to gefitinib by regulating miR-10a-5p/PTEN axis. Cell Biol Int. 2021;45:107–16.
37. Zhou Y, Zheng X, Xu B, Chen L, Wang Q, Deng H, Jiang J. Circular RNA hsa_circ_0004015 regulates the proliferation, invasion, and TKI drug resistance of non-small cell lung cancer by miR-1183/PDPK1 signaling pathway. Biochem Biophys Res Commun. 2019;508:527–35.
38. Zhang M, Bai X, Zeng X, Liu J, Liu F, Zhang Z. circRNA-miRNA-mRNA in breast cancer. Clin Chim Acta. 2021;523:120–30.
39. Chen W, Xu J, Wu Y, Liang B, Yan M, Sun C, Wang D, Hu X, Liu L, Hu W, et al. The potential role and mechanism of circRNA/miRNA axis in cholesterol synthesis. Int J Biol Sci. 2023;19:2879–96.
40. Bai S, Wu Y, Yan Y, Shao S, Zhang J, Liu J, Hui B, Liu R, Ma H, Zhang X, Ren J. Construct a circRNA/miRNA/mRNA regulatory network to explore potential pathogenesis and therapy options of clear cell renal cell carcinoma. Sci Rep. 2020;10:13659.
41. Huang S, Zou C, Tang Y, Wa Q, Peng X, Chen X, Yang C, Ren D, Huang Y, Liao Z, et al. miR-582-3p and miR-582-5p Suppress Prostate Cancer Metastasis to Bone by Repressing TGF-β Signaling. Mol Ther Nucleic Acids. 2019;16:91–104.
42. Zeng X, Ma X, Guo H, Wei L, Zhang Y, Sun C, Han N, Sun S, Zhang N. MicroRNA-582-5p promotes triple-negative breast cancer invasion and metastasis by antagonizing CMTM8. Bioengineered. 2021;12:10126–35.
43. Shu Z, Chen L, Ding D. miR-582-5P induces colorectal cancer cell proliferation by targeting adenomatous polyposis coli. World J Surg Oncol. 2016;14:239.
44. Hu Y, Su Y, Lei X, Zhao H, Wang L, Xu T, Guo J, Yang W, Zhang X. LINC00641/miR-582-5p mediate oxaliplatin resistance by activating autophagy in gastric adenocarcinoma. Sci Rep. 2020;10:14981.
45. Xu Z, Cai Y, Liu W, Kang F, He Q, Hong Q, Zhang W, Li J, Yan Y, Peng J. Downregulated exosome-associated gene FGF9 as a novel diagnostic and prognostic target for ovarian cancer and its underlying roles in immune regulation. Aging (Albany NY). 2022;14:1822–35.
46. Cui G, Shao M, Gu X, Guo H, Zhang S, Lu J, Ma H. The value of FGF9 as a novel biomarker in the diagnosis of prostate cancer. Artif Cells Nanomed Biotechnol. 2019;47:2241–5.
47. Ishioka K, Yasuda H, Hamamoto J, Terai H, Emoto K, Kim TJ, Hirose S, Kamatani T, Mimaki S, Arai D, et al. Upregulation of FGF9 in Lung Adenocarcinoma Transdifferentiation to Small Cell Lung Cancer. Cancer Res. 2021;81:3916–29.
48. Zhang Z, Zhang Y, Qin X, Wang Y, Fu J. FGF9 promotes cisplatin resistance in colorectal cancer via regulation of Wnt/β-catenin signaling pathway. Exp Ther Med. 2020;19:1711–8.
49. Li L, Zhang C, Li Y, Zhang Y, Lei Y. DJ-1 promotes epithelial-to-mesenchymal transition via enhancing FGF9 expression in colorectal cancer. Biol Open. 2020;5:bio051680.
50. Yang H, Fang F, Chang R, Yang L. MicroRNA-140-5p suppresses tumor growth and metastasis by targeting transforming growth factor β receptor 1 and fibroblast growth factor 9 in hepatocellular carcinoma. Hepatology. 2013;58:205–17.
51. Xu X, Zhang M, Xu F, Jiang S. Wnt signaling in breast cancer: biological mechanisms, challenges and opportunities. Mol Cancer. 2020;19:165.
52. Zhong Z, Virshup DM. Wnt Signaling and Drug Resistance in Cancer. Mol Pharmacol. 2020;97:72–89.
53. Zhou Y, Xu J, Luo H, Meng X, Chen M, Zhu D. Wnt signaling pathway in cancer immunotherapy. Cancer Lett. 2022;525:84–96.
54. Chen X, Liu J, Cheng L, Li C, Zhang Z, Bai Y, Wang R, Han T, Huang C, Kong Y, et al. Inhibition of noncanonical Wnt pathway overcomes enzalutamide resistance in castration-resistant prostate cancer. Prostate. 2020;80:256–66.
55. Wang W, Li M, Ponnusamy S, Chi Y, Xue J, Fahmy B, Fan M, Miranda-Carboni GA, Narayanan R, Wu J, Wu ZH. ABL1-dependent OTULIN phosphorylation promotes genotoxic Wnt/β-catenin activation to enhance drug resistance in breast cancers. Nat Commun. 2020;11:3965.

Publisher's Note